A 2D topology optimisation algorithm in NURBS framework with geometric constraints

Giulio Costa, Marco Montemurro, Jérôme Pailhès

A 2D TO algorithm in NURBS framework with geometric constraints

Giulio Costa, Marco Montemurro*, Jérôme Pailhès
Arts et Métiers ParisTech, I2M CNRS UMR 5295, F-33400 Talence, France.

This is a pre-print of an article published in *International Journal of Mechanics and Materials in Design*. The final authenticated version is available online at: https://doi.org/10.1007/s10999-017-9396-z

Corresponding author:
Marco Montemurro, PhD,
Arts et Métiers ParisTech,
I2M CNRS UMR 5295,
F-33400 Talence, France,
tel: +33 55 68 45 422,
fax: +33 54 00 06 964,
e.mail: marco.montemurro@ensam.eu,
marco.montemurro@u-bordeaux.fr

*Corresponding author.

Abstract

In this paper, the Solid Isotropic Material with Penalisation (SIMP) method for Topology Optimisation (TO) of 2D problems is reformulated in the Non-Uniform Rational BSpline (NURBS) framework. This choice implies several advantages, such as the definition of an implicit filter zone and the possibility for the designer to get a geometric entity at the end of the optimisation process. Therefore, important facilities are provided in CAD postprocessing phases in order to retrieve a consistent and well connected final topology. The effect of the main NURBS parameters (degrees, control points, weights and knot-vector components) on the final optimum topology is investigated. Classic geometric constraints, as the minimum and the maximum member size have been integrated and reformulated according to the NURBS formalism. Furthermore, a new constraint on the local curvature radius has been developed thanks to the NURBS formalism and properties. The effectiveness and the robustness of the proposed method are tested and proven through some benchmarks taken from literature and the results are compared with those provided by the classical SIMP approach.

Keywords:

Topology Optimisation; NURBS surfaces; Finite Element Method; CAD-compatibility; Structural Optimisation

1 Introduction

In the last three decades, Topology Optimisation (TO) has gained an increasing degree of interest in both academic and industrial fields. The aim of TO for structural applications is to distribute one or more material phases in a prescribed domain in order to satisfy the requirements for the problem at hand. Usually, the design problem is formulated as a Constrained Non-Linear Programming Problem (CNLPP) wherein a given cost (or objective) function must be minimised by meeting, at the same time, the full set of optimisation constraints. Classically, first TO methods were based on a Finite Elements (FE) description of the geometry [1]. The basic idea consists of defining a continuous fictitious density function varying between zero and one on the computation domain. The density function is evaluated at the centroid of each element of a predefined mesh and provides information about the topology: “void" and “solid" phases are associated to the lower and upper bounds of the density function, i.e. zero and one, respectively. Meaningless “gray" elements (related to intermediate values of the density function) are allowed but penalised during optimisation in order to achieve a “clear" solid-void design. So, mechanical properties of each element are computed (and penalised) according to the local density value. Several interpolation schemes have been developed for evaluating mechanical properties, e.g. Solid Isotropic Material with Penalisation (SIMP) or Rational Approximation of Material Properties (RAMP) [2]. Since the pioneering works on TO, different strategies were proposed during the years in order to overcome classic TO drawbacks, such as checker-board effect and mesh dependence. Projection methods have been used in [3] and their robustness has been investigated in [4]. These algorithms, based on projection and suitable filters, exhibit fine features since they integrate specific geometric constraints [5]. Density-based TO methods are really efficient and can be implemented in very compact scripts [6]. However,

in spite of their relative simplicity, they provide a FE-based description of the final geometry and suitable postprocessing must be forecast in order to obtain a smooth CAD-compatible design. A different TO method, originated from the exigence of precisely controlling the boundaries of the optimised structure, is referred in literature as Level Set Method (LSM) [7]. A FE model is utilised only to describe the physics of the problem at hand, whilst the topology of the system is represented through a suitable Level Set Function (LSF). In the 3D case, the LSF is a scalar function, defined in $\mathrm{I} \subset \mathbb{R}$, which represents the image of the generic point ($P = \{x, y, z, t\}$) belonging to the domain $\mathrm{D} \subset \mathbb{R}^4$. The sign of the LSF can be conventionally associated to material or void zones while the zero value represents the boundary of the optimised structure [8]. Furthermore, the evolution of the boundary of the domain (i.e. the zero value of the LSF) is governed by the Hamilton-Jacobi Equation and represents its fundamental solution. The LSM is characterised by two main advantages:

a) the LSF gives a clear implicit geometric representation of the boundary of the domain;

b) unlike density-based methods, the LSF is not affected by greyness effect.

A thorough discussion on the LSM for structural TO applications can be found in [9]. The LSF can be chosen among different sets of functions, according to local or global support, dimension of the local support, mathematical nature of the function [10]. Often, Radial Basis Functions (RBFs) are utilised because of their versatility and simplicity [11, 12, 13].

Recent efforts are finalised to fill in some gaps of current TO methods. In particular, the main shortcoming of density-based strategies is the time consuming postprocessing phase necessary to rebuild the boundaries of the optimum topology of the structure starting from a FE "pixelised" domain (providing the required smoothness). The LSM represents a first attempt to overcome this difficulty by introducing geometric entities to properly describe the topology. In the procedure discussed in [14], the LSM is coupled to the isogeometric analysis by means of Non-Uniform Rational BSpline (NURBS) formalism for both LSF parametrisation and objective function computation. However, the LSM is not free from drawbacks. Tipically, the LSM is based on the Hamilton-Jacobi equation, that needs particular attention to be solved: it should be properly reinitialised and the Courant-Friedrichs-Lewy condition must be met to satisfy specific requirements on the time step related to the mesh dimension [7]. Moreover, the LSM is affected by the initial topology of the domain (i.e. the initial guess) and, roughly speaking, when considering the classical formulation based on the shape derivative, holes can merge but cannot nucleate in the structure [9]. Such a sensitivity of the solution to the initial guess of the topology can be eliminated by means of the topological derivative and a fictitious energetic term in the objective function [15]. Unfortunately, solutions exhibit a dependence on the weight parameter of the energetic term in the objective function. As far as concerns density-based TO methods, a first enhancement was presented in [16] by relating the fictitious density function to a BSpline surface for 2D TO problems. The main advantages of this choice were the implicit filter zone and the mesh-independence of the solution.

However, any development was introduced about the handling of geometric constraints and the improvement of the postprocessing phase required to get a CAD-compatible shape.

Providing a careful description of the geometry is crucial in TO not only to save time in postprocessing but, mostly, to ensure that the optimum shape of the component (rebuilt at the end of TO) could meet the design constraints. Nowadays, commercial software like OptiStruct (a module of Altair HyperWorks package) [17] or Tosca (a module of Abaqus Package) [18] are widely utilised in industrial field. Since they make use of a density-based method, suitable tools are needed to rebuild the boundary of the optimum topology. Although these tools are quite fast and efficient, usually the rebuilt geometry does not satisfy part (or the full set) of the design constraints considered for the problem at hand.

Typical constraints account for the control of geometric features on the one hand and manufacturing requirements on the other hand. Some constraints can concern both aspects, like the constraints on the local thickness (referred in literature as *minimum and maximum member size*) of topological branches appearing during optimisation. The minimum member size can be taken into account in density-based TO algorithms through a simple criterion on the monotonicity of the fictitious density function along n search directions: typically $n = 4$ and $n = 13$ for the 2D and 3D case, respectively [19]. It has been proven that this constraint constitutes also an implicit filter that can replace classical distance-based filters in order to prevent the checker-board effect in density-based TO methods. Further strategies to account for the minimum member size in density-based TO methods make use of projection and filtering techniques, see [3] and [20]. Also the *dilated* and *eroded* description of the topology outlined in [21] finally results in an implicit control on the minimum member size. An efficient way of handling the maximum member size constraint is presented in [5], while explicit constraints on the members dimensions can be directly imposed in the framework of the LSM by introducing the 'skeleton" concept, see [22] and [23].

Considering all of the previous aspects, in this paper an alternative density-based TO method for 2D problems is presented. Taking inspiration from the work of [16], the proposed method is based on the utilisation of the NURBS formalism (in the context of the SIMP approach) to represent the fictitious density function that becomes a NURBS surface (for 2D problems). Each point of the NURBS control net is then characterised by three coordinates of which two are Cartesian coordinates and the third one is the density. The proposed approach, also called NURBS-based SIMP approach [24], is characterised by several original features which make it a general and efficient methodology for dealing with 2D topology optimisation problems. Thanks to the NURBS formalism, the proposed methodology is fully compatible with CAD software. The method is extremely versatile and all the classical geometric constraints (minimum and maximum member size, symmetries, etc.) can be easily reformulated by means of the NURBS surfaces. Furthermore, since the NURBS formalism gives an exact representation of the boundary of the structure, a new geometric constraints on the local curvature radius of the boundary has been formulated and implemented. Finally, unlike the work of [16], the influence of the weights on the optimum topology

has been taken into account and a relevant sensitive analysis has been carried out.

Some benchmarks, taken from literature [2, 5], are considered to prove the the effectiveness of the NURBS-based SIMP method.

The paper is structured as follows: firstly, the theoretical framework of both NURBS surfaces and SIMP method is presented. Then, the mathematical formulation of the proposed methodology is given in Section 3. In Section 4, the mathematical formulation of geometric constraints is outlined together with the related gradient computation. The numerical strategy is then briefly described in Section 5. Section 6 is dedicated to the discussion of meaningful results and, finally, Section 7 ends the paper with some conclusions and perspectives.

2 Theoretical framework

In this Section, the fundamental concepts and notations of the NURBS theory and SIMP TO method are briefly recalled.

2.1 The NURBS surface theory

According to the notation of [25], a NURBS surface is defined as:

$$\mathbf{S}(u,v) = \sum_{i=0}^{n_u} \sum_{j=0}^{n_v} R_{i,j}(u,v)\mathbf{P}_{i,j}, \tag{1}$$

where $R_{i,j}(u,v)$ are the piecewise rational basis functions, which are related to the standard NURBS blending functions $N_{i,p}(u)$ and $N_{j,q}(v)$ by means of the relationship

$$R_{i,j}(u,v) = \frac{N_{i,p}(u)N_{j,q}(v)w_{i,j}}{\sum_{k=0}^{n_u}\sum_{l=0}^{n_v} N_{k,p}(u)N_{l,q}(v)w_{k,l}}. \tag{2}$$

In Eqs. (1) and (2), $\mathbf{S}(u,v)$ is a bivariate vector-valued piecewise rational function, (u,v) are scalar dimensionless parameters both defined in the interval $[0,1]$, while p and q are the NURBS degrees along u and v directions, respectively; $w_{i,j}$ are the weights and $\mathbf{P}_{i,j} = \{x_{i,j}, y_{i,j}, z_{i,j}\}$ the Cartesian coordinates of the generic control point, with $i = 0, ..., n_u$ and $j = 0, ..., n_v$. The net of $(n_u + 1) \times (n_v + 1)$ control points constitutes the so-called *control net*. The blending functions are recursively defined by means of the Bernstein's polynomials:

$$N_{i,0}(u) = \begin{cases} 1 \text{ if } U_i \leq u < U_{i+1}, \\ 0 \text{ otherwise}, \end{cases} \tag{3}$$

$$N_{i,p}(u) = \frac{u - U_i}{U_{i+p} - U_i} N_{i,p-1}(u) + \frac{U_{i+p+1} - u}{U_{i+p+1} - U_{i+1}} N_{i+1,p-1}(u), \tag{4}$$

where U_i is the i-th component of the following non-periodic non-uniform *knot vector*:

$$\mathbf{U} = \{\underbrace{0, \ldots, 0}_{p+1}, U_{p+1}, \ldots, U_{m_u-p-1}, \underbrace{1, \ldots, 1}_{p+1}\}. \tag{5}$$

It is noteworthy that the size of the knot vector is $m_u + 1$,

$$m_u = n_u + p + 1. \tag{6}$$

Analogously, the $N_{j,q}(v)$ are defined on the knot vector $\mathbf{V}$, whose size is m_v:

$$\mathbf{V} = \{\underbrace{0, \ldots, 0}_{q+1}, V_{q+1}, \ldots, V_{m_v-q-1}, \underbrace{1, \ldots, 1}_{q+1}\}, \tag{7}$$

$$m_v = n_v + q + 1. \tag{8}$$

The knot vectors $\mathbf{U}$ and $\mathbf{V}$ are two non-decreasing sequences of real numbers that can be interpreted as two discrete collections of values of the dimensionless parameters u and v. As the control points, also the knot vectors components form a net. One basic property of the blending functions is the *local support property*: $N_{i,p}(u) = 0$ if u is outside the interval $[U_i, U_{i+p+1}[$. Hence, it is evident that $R_{i,j}(u, v) = 0$ if (u, v) is outside the rectangle $[U_i, U_{i+p+1}[\times[V_j, V_{j+q+1}[$, i.e. the local support associated to the control point $\mathbf{P}_{i,j}$. The local support property is of paramount importance to understand all the advantages of the NURBS formulation of the SIMP method in the context of TO. For a deeper insight in the NURBS theory, the reader is addressed to [25].

2.2 The classic SIMP method

The SIMP method is briefly discussed here for the minimum compliance 2D problem subject to an equality constraint on the volume [2]. Let us consider a rectangular reference domain $D \subset \mathbb{R}^2$ in a Cartesian orthogonal frame $O(x, y)$. Let D be defined as

$$D = \{(x, y) \in \mathbb{R}^2 | x \in [0, W], y \in [0, H]\}, \tag{9}$$

where W and H are two reference lengths of the domain (that can vary depending to the considered problem) along x and y axes, respectively. The goal is to find the optimal distribution of a given isotropic material on D by minimising the compliance (i.e. the virtual work of external applied loads) with an imposed volume fraction f of the design domain. The material distribution (void and material zones) affects the stiffness tensor $E_{ijkl}(\mathbf{x})$, which is variable over the domain D. Let $\Omega \subseteq D$ be the material domain. In the SIMP approach, Ω is determined by means of a fictitious density function $\rho(\mathbf{x}) \in [0, 1]$ defined over the whole design domain D. Such a density field is related to the material distribution: $\rho(\mathbf{x}) = 0$ means absence of material, whilst $\rho(\mathbf{x}) = 1$ implies completely dense base material. The relationship between the stiffness tensor $E_{ijkl}(\mathbf{x})$ and the density field $\rho(\mathbf{x})$ is

$$E_{ijkl}(\rho(\mathbf{x})) = \rho(\mathbf{x})^\alpha E^0_{ijkl}, \tag{10}$$

where E^0_{ijkl} is the stiffness tensor of the isotropic material and $\alpha \geq 3$ a suitable parameter that aims at penalising all the meaningless densities between 0 and 1. Let $\mathbf{u}$ be the displacement vector

field and $l(\mathbf{u})$ the compliance of the structure, namely

$$l(\mathbf{u}) = \int_D \rho(\mathbf{x})^\alpha E^0_{ijkl} \varepsilon_{ij}(\mathbf{u}) \varepsilon_{kl}(\mathbf{u}) dD. \tag{11}$$

In Eq. (11), ε_{ij} $(i,j = 1,2,3)$ are the components of the strain tensor. The FEM-discretised version of Eq. (11) is:

$$c = \{\mathrm{U_{FEM}}\}^T [\mathrm{K}] \{\mathrm{U_{FEM}}\} \ , \tag{12}$$

where [K] is the global stiffness matrix of the structure defined as

$$[\mathrm{K}] = \sum_{e=1}^{N_e} \rho_e^\alpha [\mathrm{K}_e] \ . \tag{13}$$

In Eq. (12), $\{\mathrm{U_{FEM}}\}$ is the vector of the degrees of freedom (DOFs), also called nodal generalised displacements, of the structure representing the solution of the problem:

$$[\mathrm{K}] \{\mathrm{U_{FEM}}\} = \{\mathrm{F}\} \ , \tag{14}$$

wherein $\{\mathrm{F}\}$ is the vector of the nodal generalised external forces. In Eq. (13), ρ_e is the fictitious density computed at the centroid of the generic element e, whilst $[\mathrm{K}_e]$ is the non-penalised element stiffness matrix expanded over the full set of DOFs of the structure. The problem of determining the optimum topology which minimises the compliance subject to a constraint on the overall volume can be stated as follow:

$$\begin{aligned} &\min_{\rho_e} \ \ c(\rho_e), \\ &\text{subject to:} \\ &\begin{cases} [\mathrm{K}]\{\mathrm{U}_{FEM}\} = \{\mathrm{F}\}, \\ \dfrac{V(\rho_e)}{V_{tot}} = \dfrac{\sum_{e=1}^{N_e} \rho_e A_e}{WH} = f, \\ \rho_{min} \leq \rho_e \leq 1, \quad e = 1, ..., N_e. \end{cases} \end{aligned} \tag{15}$$

In Eq. (15), V_{tot} is the overall volume of the definition domain D, $V(\rho_e)$ is the volume of the material domain Ω, while f is the fixed volume fraction; A_e is the area of element e on the $x-y$ plane and ρ_{min} represents the lower bound imposed to the density field in order to prevent any singularity for the solution of the equilibrium problem.

It must be pointed out that the SIMP method can lead to numerical issues, e.g. the well-known checker-board effect, related to the lack of mutual dependency among the design variables, i.e. the pseudo-densities ρ_e defined at each element centroid. To repair these issues, a distance-based filter is usually employed [2]. For the sake of completeness, the derivative of the compliance with respect to the elements fictitious densities can be deduced by means of the adjoins method [2]:

$$\frac{\partial c}{\partial \rho_e} = -\alpha \rho_e^{\alpha-1} \{\mathrm{U}_{FEM}\}^T [\mathrm{K}_e] \{\mathrm{U}_{FEM}\}, \ e = 1, ..., N_e. \tag{16}$$

Moreover, Eq. (16) can be simplified by defining the compliance of the single element:

$$c_e = \rho_e^{\alpha} \{\mathrm{U}_{FEM}\}^T [\mathrm{K}_e] \{\mathrm{U}_{FEM}\}. \tag{17}$$

Thus, the sensitivity analysis for the compliance finally writes:

$$\frac{\partial c}{\partial \rho_e} = -\frac{\alpha}{\rho_e} c_e, \ e = 1, ..., N_e. \tag{18}$$

The sensitivity of the volume fraction is

$$\frac{1}{V_{tot}} \frac{\partial V}{\partial \rho_e} = \frac{A_e}{WH}, \ e = 1, ..., N_e. \tag{19}$$

3 The NURBS-based SIMP method: mathematical formulation

In the framework of the proposed approach, the pseudo-density field characterising the SIMP method is related to a suitable NURBS scalar function:

$$\rho(u, v) = \sum_{i=0}^{n_u} \sum_{j=0}^{n_v} R_{i,j}(u, v) \overline{\rho}_{i,j}. \tag{20}$$

The shape of the NURBS is affected by the value of the fictitious density at each control point, i.e. $\overline{\rho}_{i,j}$, as well as by the value of the other parameters involved into the definition of the NURBS scalar function, namely the degrees of the blending function, i.e. p and q, the number of control points $(n_u + 1) \times (n_v + 1)$, the weights $w_{i,j}$ and the value of the knot vectors components, as illustrated in Eqs. (2) and (4). The dimensionless parameters u and v can be arbitrarily defined. For 2D TO problems, the most intuitive choice is to relate them to the Cartesian coordinates of the global frame as:

$$\begin{cases} u = \frac{x}{W}, \\ v = \frac{y}{H}. \end{cases} \tag{21}$$

In Eq. (20), the control points $\overline{\rho}_{i,j}$ and the weights $w_{i,j}$ are the design variables of the NURBS-based SIMP method. They are collected in two column arrays $\boldsymbol{\xi}$ and $\boldsymbol{\eta}$. Suitable boundaries are imposed to satisfy the density field requirements for the TO problem:

$$\begin{aligned} &\boldsymbol{\xi} = \{\overline{\rho}_{0,0}, ..., \overline{\rho}_{n_u,0}, \overline{\rho}_{0,1}, ..., \overline{\rho}_{n_u,1}, ..., \overline{\rho}_{0,n_v}, ..., \overline{\rho}_{n_u,n_v}\}, \\ &\overline{\rho}_{i,j} \in [\rho_{min}, 1], \quad \forall i = 0, ..., n_u, \quad \forall j = 0, ..., n_v. \end{aligned} \tag{22}$$

$$\begin{aligned} &\boldsymbol{\eta} = \{w_{0,0}, ..., w_{n_u,0}, w_{0,1}, ..., w_{n_u,1}, ..., w_{0,n_v}, ..., w_{n_u,n_v}\}, \\ &w_{i,j} \in [w_{min}, w_{max}], \ w_{min}, w_{max} \in \mathbb{R}, \ \forall i = 0, ..., n_u, \ \forall j = 0, ..., n_v. \end{aligned} \tag{23}$$

Without loss of generality, in this work the two knot vectors $\mathbf{U}$ and $\mathbf{V}$ are considered uniformly distributed in the interval $[0, 1]$ and both the degrees of the blending functions and the number of

control points are fixed *a priori*. In this background, the 2D TO problem can be stated as:

$$\begin{aligned}
&\min_{\boldsymbol{\xi},\boldsymbol{\eta}} \; c(\rho(\boldsymbol{\xi},\boldsymbol{\eta})),\\
&\text{subject to:}\\
&\begin{cases}
(\sum_{e=1}^{N_e} \rho_e^{\alpha}[\mathrm{K}_e])\{\mathrm{U}_{FEM}\} = [\mathrm{K}]\{\mathrm{U}_{FEM}\} = \{\mathrm{F}\},\\
\dfrac{V(\rho_e)}{V_{tot}} = \dfrac{\sum_{e=1}^{N_e} \rho_e A_e}{WH} = f,\\
\{\mathrm{g}(\boldsymbol{\xi},\boldsymbol{\eta})\} \leq \{0\},\\
\xi_k \in [\rho_{min}, 1],\\
\eta_k \in [w_{min}, w_{max}],\\
\forall k = 1, ..., (n_u+1)\times(n_v+1).
\end{cases}
\end{aligned} \tag{24}$$

In Eq. (24), $\{\mathrm{g}(\boldsymbol{\xi},\boldsymbol{\eta})\}$ is the vector collecting the constraints of different nature (geometric, technological or physical), whilst ρ_e is the value of the pseudo-density for the generic element,

$$\rho_e = \rho(u_e, v_e) = \rho\left(\frac{x_e}{W}, \frac{y_e}{H}\right), \tag{25}$$

where (x_e, y_e) are the Cartesian coordinates of the element centroid.

The new formulation implies two new variables sets, different from the element densities, so a sensitivity analysis should be carried out. It can be proven (see Appendix A) that the derivatives of both the compliance and the volume with respect to the fictitious density at each control point can be expressed as

$$\frac{\partial c}{\partial \overline{\rho_{s,t}}} = -\alpha \sum_{e \in I_{s,t}} \frac{c_e}{\rho_e} R_{s,t}(u_e, v_e), \tag{26}$$

$$\frac{1}{V_{tot}} \frac{\partial V}{\partial \overline{\rho_{s,t}}} = \frac{1}{WH} \sum_{e \in I_{s,t}} A_e R_{s,t}(u_e, v_e), \tag{27}$$

while for the weights

$$\frac{\partial c}{\partial w_{s,t}} = -\frac{\alpha}{w_{s,t}} \sum_{e \in I_{s,t}} c_e \frac{\overline{\rho_{s,t}} - \rho_e}{\rho_e} R_{s,t}(u_e, v_e), \tag{28}$$

$$\frac{1}{V_{tot}} \frac{\partial V}{\partial w_{s,t}} = \frac{1}{WHw_{s,t}} \sum_{e \in I_{s,t}} A_e (\overline{\rho_{s,t}} - \rho_e) R_{s,t}(u_e, v_e). \tag{29}$$

In Eqs. (26)-(29), $I_{s,t}$ represents the local support related to the generic control point [25]. Once the sensitivity analysis has been provided, a suitable gradient-based algorithm can be utilised as a tool for the solution search of problem (24).

The SIMP approach revisited in the NURBS mathematical framework is characterised by the following features (which implies just as many advantages):

1. The number of design variables is unrelated to the number of elements. In the classic SIMP approach, each element introduces a new design variable. In the NURBS framework, the accuracy of the topology description is characterised solely by the number of points of the control net, i.e. $(n_u+1)\times(n_v+1)$;

2. The *local support property* of the NURBS blending functions defines an implicit filter zone. The size of such a filter zone is related to the dimensions of the local support of the blending functions, i.e. to the components of the knot vectors as well as to the degrees of the basis functions. It should be remarked that TO filters create a mutual dependency area among the elements densities, i.e. the design variables in standard SIMP formulations. In the case of NURBS, the inter-dependence is automatically provided thanking the NURBS local support, without the need of defining a filter on the mesh elements densities.

3. The NURBS formalism allows taking into account a wide constraints gamma, since a mathematically well-defined description of the geometrical bounds of the optimum topology is always available during the iterations of the optimisation process. Nevertheless, local information, such as the local normal and tangent vectors, can be easily deduced from standard NURBS formulae.

4 Geometrical constraints: mathematical formulation

In this Section, two classical geometric constraints in TO, i.e. the minimum and maximum members size, as well as a new constraint on the local curvature radius will be formulated in the mathematical framework of the proposed NURBS-based SIMP approach. They will constitute the components of the constraint vector $\{\mathrm{g}(\boldsymbol{\xi}, \boldsymbol{\eta})\}$ appearing in the CNLPP (24).

4.1 Minimum Member Size

The minimum member size constraint is used in TO to provide a minimum admissible size of structural elements. Here, the formulation proposed by [19] is considered. The intuitive idea consists of imposing the monotonicity of the fictitious density function in a circular area having a diameter equal to the minimum member size (d_{min}). The circular area is sketched around each mesh element and the monotonicity is checked every time along four directions (0°, 90°, ±45°). Mathematically speaking, the monotonicity of a function on an interval I along a direction $\boldsymbol{\gamma}$ can be checked by means of the following integral:

$$M_{\boldsymbol{\gamma}}(f) = \int_I |\nabla f \cdot \boldsymbol{\gamma}| - |\int_I \nabla f \cdot \boldsymbol{\gamma}|. \tag{30}$$

$M_{\boldsymbol{\gamma}}(f)$ is strictly equal to 0 if f is monotone and grater than 0 otherwise. Therefore, the constraint on the minimum member size is formulated as follows:

$$g_{d_{min}} = \sum_{e=1}^{N_e} \left(\sum_{\boldsymbol{\gamma}_i} M_{\boldsymbol{\gamma}_i}(\rho) \right)^{\theta} - \sigma \leq 0, \tag{31}$$

where N_e is the number of mesh elements, $\boldsymbol{\gamma}_i$ the checking direction ($i = 1, ..., 4$), θ a penalising exponent and σ is used to relax the constraint and to provide numerical stability. Of course, $M_{\boldsymbol{\gamma}_i}(\rho)$

is the monotonicity integral and its evaluation domain is the circular zone having diameter d_{min} and centred at the centroid of each element. The explicit expression of $M_{\boldsymbol{\gamma}_i}(\rho)$ is

$$M_{\boldsymbol{\gamma}_i}(\rho) = \int_{-d_{min}/2}^{d_{min}/2} |\nabla\rho \cdot \boldsymbol{\gamma}_i| ds - \left| \int_{-d_{min}/2}^{d_{min}/2} \nabla\rho \cdot \boldsymbol{\gamma}_i ds \right|. \tag{32}$$

In Eq. (32), s is a suitable abscissa along the current checking direction $\boldsymbol{\gamma}_i$. In particular, $\boldsymbol{\gamma}_1 = [1,0]^t$, $\boldsymbol{\gamma}_2 = [0,1]^t$, $\boldsymbol{\gamma}_3 = [\sqrt{2}/2, \sqrt{2}/2]^t$ and $\boldsymbol{\gamma}_4 = [\sqrt{2}/2, -\sqrt{2}/2]^t$. In order to formulate a discrete version of Eq. (32), let us consider a regular *mapped* mesh of square elements. Then, $N_{\boldsymbol{\gamma}_i}$ is the number of mesh elements spanning the diameter d_{min} along $\boldsymbol{\gamma}_i$ direction. It is straightforward to verify (see [19]) that Eq. (32) changes into

$$M_{\boldsymbol{\gamma}_i}(\rho) = \sum_{j=1}^{N_{\boldsymbol{\gamma}_i}-1} |\rho_{j+1} - \rho_j| - \left|\rho_{N_{\boldsymbol{\gamma}_i}} - \rho_1\right|. \tag{33}$$

It is remarked that j in Eq. (33) is just a mute index that sweeps the interval $[0, d_{min}]$, like the abscissa s in Eq. (32). Furthermore, a smooth approximation of the absolute function has been employed to regularise the constraint evaluation for the gradient based algorithm, namely

$$|z| \approx \sqrt{z^2 + \epsilon^2} - \epsilon, \tag{34}$$

with $\epsilon = 0.01$. The final expression of $M_{\boldsymbol{\gamma}_i}(\rho)$ to be implemented is

$$M_{\boldsymbol{\gamma}_i}(\rho) = \sum_{j=1}^{N_{\boldsymbol{\gamma}_i}-1} \left(\sqrt{(\rho_{j+1} - \rho_j)^2 + \epsilon^2} - \epsilon \right) - \sqrt{(\rho_{N_{\boldsymbol{\gamma}_i}} - \rho_1)^2 + \epsilon^2} + \epsilon. \tag{35}$$

As far as the sensitivity analysis is concerned, the derivative of the minimum member size constraint with respect to the NURBS control points writes:

$$\frac{\partial g_{d_{min}}}{\partial \overline{\rho_{s,t}}} = \theta \sum_{e=1}^{N_e} \left(\sum_{\boldsymbol{\gamma}_i} M_{\boldsymbol{\gamma}_i}(\rho) \right)^{\theta-1} \left(\sum_{\boldsymbol{\gamma}_i} \frac{\partial M_{\boldsymbol{\gamma}_i}(\rho)}{\partial \overline{\rho_{s,t}}} \right). \tag{36}$$

Analogously, the derivative with respect to the NURBS weights is

$$\frac{\partial g_{d_{min}}}{\partial w_{s,t}} = \theta \sum_{e=1}^{N_e} \left(\sum_{\boldsymbol{\gamma}_i} M_{\boldsymbol{\gamma}_i}(\rho) \right)^{\theta-1} \left(\sum_{\boldsymbol{\gamma}_i} \frac{\partial M_{\boldsymbol{\gamma}_i}(\rho)}{\partial w_{s,t}} \right). \tag{37}$$

The only difficult consists in evaluating the terms $\dfrac{\partial M_{\boldsymbol{\gamma}_i}(\rho)}{\partial \overline{\rho_{s,t}}}$ and $\dfrac{\partial M_{\boldsymbol{\gamma}_i}(\rho)}{\partial w_{s,t}}$. The detailed computation is carried out in Appendix B and the final result is provided here:

$$\begin{aligned} \frac{\partial M_{\boldsymbol{\gamma}_i}(\rho)}{\partial \overline{\rho_{s,t}}} = \sum_{j=1}^{N_{\boldsymbol{\gamma}_i}-1} \frac{(\rho_{j+1} - \rho_j)\left(R_{s,t}(u_{j+1}, v_{j+1}) - R_{s,t}(u_j, v_j)\right)}{\sqrt{(\rho_{j+1} - \rho_j)^2 + \epsilon^2}} + \\ - \frac{(\rho_{N_{\boldsymbol{\gamma}_i}} - \rho_1)\left(R_{s,t}(u_{N_{\boldsymbol{\gamma}_i}}, v_{N_{\boldsymbol{\gamma}_i}}) - R_{s,t}(u_1, v_1)\right)}{\sqrt{(\rho_{N_{\boldsymbol{\gamma}_i}} - \rho_1)^2 + \epsilon^2}}, \end{aligned} \tag{38}$$

$$\frac{\partial M_{\gamma_i}(\rho)}{\partial w_{s,t}} = \frac{\overline{\rho_{s,t}}}{w_{s,t}} \frac{\partial M_{\gamma_i}(\rho)}{\partial \overline{\rho_{s,t}}} + \\ + \frac{1}{w_{s,t}} \left[\sum_{j=1}^{N_{\gamma_i}-1} \frac{(\rho_{j+1}-\rho_j)\left(\rho_j R_{s,t}(u_j,v_j) - \rho_{j+1} R_{s,t}(u_{j+1},v_{j+1})\right)}{\sqrt{(\rho_{j+1}-\rho_j)^2+\epsilon^2}} + \right. \\ \left. - \frac{(\rho_{N_{\gamma_i}}-\rho_1)\left(\rho_1 R_{s,t}(u_1,v_1) - \rho_{N_{\gamma_i}} R_{s,t}(u_{N_{\gamma_i}},v_{N_{\gamma_i}})\right)}{\sqrt{(\rho_{N_{\gamma_i}}-\rho_1)^2+\epsilon^2}} \right]. \tag{39}$$

In Eqs. (38) and (39), it is assumed $\rho_j = \rho(u_j, v_j)$.

4.2 Maximum Member Size

The maximum member size is used in TO in order to limit the maximum thickness of topological elements. Using the maximum and the minimum member size simultaneously is a smart choice to obtain structures with uniform dimensions. This aspect could be particularly advantageous in additive manufacturing production in order to avoid residual stresses in the final structure: in fact, a relevant difference in structural members size implies a difference in the amount of exposed surface (thinner elements will chill faster than massive parts), thus leading to a non-uniform heat exchange. Consequently, the occurring temperature gradient will constitute one of the most important causes of residual stresses, see [26]. In this work, Guest's formulation [5] has been revisited by making use of NURBS. The procedure is not so far from that proposed by Poulsen for the minimum member size. However, the constraint does not concern the monotonicity of the fictitious density function but is explicitly imposed on the material phase: in fact, a checking circular region is drawn around each element centroid (whose diameter d_{max} is equal to the desired maximum member size). Let Ω_e be the circular region; thus, the following condition must be met for each element in a 2D structure:

$$\sum_{i \in \Omega_e} \hat{\rho}_i A_i \leq \frac{\pi d_{max}^2}{4}(1-\psi), \forall e. \tag{40}$$

In Eq. (40), i is a mute index to indicate the elements in the circular zone Ω_e (built around element e), ψ is a relaxing parameter ($\psi = 0.05$), A_i is the area of element i and $\hat{\rho}_i$ is the projected fictitious density function. In this work, such a projection is performed through the relation

$$\hat{\rho_e} = \rho_e^{\alpha}, \tag{41}$$

where α is the same parameter used for the penalisation of the SIMP, refer to Eq. (10). Of course, it is not possible to impose a constraint for each mesh element and a suitable aggregation strategy must be provided. A simple sum is not recommended here because of compensatory effects. Let

a_e be the left term of Eq. (40), so

$$a_e = \sum_{i \in \Omega_e} \hat{\rho}_i A_i. \tag{42}$$

An efficient aggregation technique consists of choosing the maximum value of a among the mesh elements and making use of it in the formulation of the maximum member size constraint. However, in order to insert the maximum operator in a gradient-based algorithm, a suitable smooth approximation should be given:

$$a_{max} = \left(\sum_{e=1}^{N_e} a_e^{\chi} \right)^{\frac{1}{\chi}}, \tag{43}$$

wherein χ is a tuning parameter whose value should be big enough. Therefore, the constraint is formulated by combining Eq. (40) with Eq. (43):

$$a_{max} = \left(\sum_{e=1}^{N_e} \left(\sum_{i \in \Omega_e} \hat{\rho}_i A_i \right)^{\chi} \right)^{\frac{1}{\chi}} \leq \frac{\pi d_{max}^2}{4}(1 - \psi). \tag{44}$$

Then, Eq. (44) is arranged in order to be dimensionless and put in the form of a standard inequality constraint for the CNLPP (24) as follow

$$g_{d_{max}} = \frac{\left(\sum_{e=1}^{N_e} \left(\sum_{i \in \Omega_e} \hat{\rho}_i A_i \right)^{\chi} \right)^{\frac{1}{\chi}}}{\frac{\pi d_{max}^2}{4}(1 - \psi)} - 1 \leq 0. \tag{45}$$

It is remarked that the χ parameter has been chosen $\chi = 10$ at the beginning of the iterations and it is increased up to 35 by a continuation method.

In this case, the sensitivity analysis with respect to the NURBS control points and weights is straightforward (see Appendix B for mathematical passages):

$$\frac{\partial g_{d_{max}}}{\partial \overline{\rho_{s,t}}} = \alpha(g_{d_{max}} + 1) \frac{\sum_{e=1}^{N_e} \left(\left(\sum_{i \in \Omega_e} \rho_i^{\alpha} A_i \right)^{\chi - 1} \left(\sum_{i \in \Omega_e} \rho_i^{\alpha - 1} R_{s,t}(u_i, v_i) A_i \right) \right)}{\sum_{e=1}^{N_e} \left(\sum_{i \in \Omega_e} \hat{\rho}_i A_i \right)^{\chi}}, \tag{46}$$

$$\begin{aligned} \frac{\partial g_{d_{max}}}{\partial w_{s,t}} = & \frac{\overline{\rho_{s,t}}}{w_{s,t}} \frac{\partial g_{d_{max}}}{\partial \overline{\rho_{s,t}}} + \\ & - \frac{\alpha(g_{d_{max}} + 1)}{w_{s,t}} \frac{\sum_{e=1}^{N_e} \left(\left(\sum_{i \in \Omega_e} \rho_i^{\alpha} A_i \right)^{\chi - 1} \left(\sum_{i \in \Omega_e} \rho_i^{\alpha} R_{s,t}(u_i, v_i) A_i \right) \right)}{\sum_{e=1}^{N_e} \left(\sum_{i \in \Omega_e} \hat{\rho}_i A_i \right)^{\chi}}. \end{aligned} \tag{47}$$

4.3 Local Curvature Radius

This kind of constraint has an interest for functional and manufacturing requirements. Ideally, if the boundary of the structure is mathematically defined, the local radius of curvature can be evaluated and its minimum value can be identified. Then, the minimum value of the curvature radius can be constrained to be superior to an admissible reference value. In the framework of classical SIMP approach, it is not possible to formulate this kind of constraints since the boundary of the structure is not defined (nor in implicit neither in explicit way). Conversely, in the context of the NURBS formulation, a description of the boundary is available at each iteration by establishing a cutting plane for the NURBS surface representing the fictitious density function. Let $\Omega \subseteq D$ be the material domain and $\rho_{cut} \in [\rho_{min}, 1]$ the threshold cutting value for the density field. In order to have a precise description of the contour, it can be assumed that

$$\begin{cases} (x,y) \in \Omega, \text{ if } \rho(x,y) > \rho_{cut}, \\ (x,y) \in \partial\Omega, \text{ if } \rho(x,y) = \rho_{cut}, \\ (x,y) \in D \setminus \Omega, \text{ if } \rho(x,y) < \rho_{cut}. \end{cases} \tag{48}$$

For an implicit 2D curve, the expression of the curvature writes [27]

$$\kappa = -\frac{\left\{\frac{\partial\rho}{\partial y} \quad -\frac{\partial\rho}{\partial x}\right\}\begin{bmatrix}\frac{\partial^2\rho}{\partial x^2} & \frac{\partial^2\rho}{\partial x\partial y}\\ \frac{\partial^2\rho}{\partial x\partial y} & \frac{\partial^2\rho}{\partial y^2}\end{bmatrix}\begin{Bmatrix}\frac{\partial\rho}{\partial y}\\ -\frac{\partial\rho}{\partial x}\end{Bmatrix}}{\left(\left(\frac{\partial\rho}{\partial x}\right)^2+\left(\frac{\partial\rho}{\partial y}\right)^2\right)^{\frac{3}{2}}}. \tag{49}$$

Similarly to the minimum member size constraint, the derivatives can be arranged through the NURBS notation, so the curvature radius can be achieved:

$$r = -\frac{1}{WH}\frac{\left(H^2\left(\frac{\partial\rho}{\partial u}\right)^2+W^2\left(\frac{\partial\rho}{\partial v}\right)^2\right)^{\frac{3}{2}}}{\left(\frac{\partial\rho}{\partial u}\right)^2\frac{\partial^2\rho}{\partial v^2}-2\frac{\partial\rho}{\partial u}\frac{\partial\rho}{\partial v}\frac{\partial^2\rho}{\partial u\partial v}+\left(\frac{\partial\rho}{\partial v}\right)^2\frac{\partial^2\rho}{\partial u^2}}. \tag{50}$$

Hence, the constraint can be formulated as

$$\min_{\partial\Omega} |r(x,y)| \geq \overline{r}. \tag{51}$$

The absolute value is approximated by means of Eq. (34), whilst the minimum operator has been estimated through the Kreisselmeier-Steinhauser function [28]. Let N_r be the number of radius evaluation on the contour of the structure. Eq. (51) changes into the following relation:

$$g_r = 1 + \frac{1}{\overline{r}\tau} ln\left(\sum_{k=1}^{N_r} exp\left(-\tau(\sqrt{r_k^2+\epsilon^2}-\epsilon)\right)\right) \leq 0, \tag{52}$$

where τ should be big enough.

The derivatives of the constraint on the local curvature radius with respect to design variables (control points and weights) can be expressed as follows:

$$\frac{\partial g_r}{\partial \rho_{s,t}} = -\frac{1}{\overline{r}} \frac{\sum_{k=1}^{N_r} \frac{exp\left(-\tau(\sqrt{r_k^2+\epsilon^2}-\epsilon)\right) r_k \frac{\partial r_k}{\partial \rho_{s,t}}}{\sqrt{r_k^2+\epsilon^2}}}{\sum_{k=1}^{N_r} exp\left(-\tau(\sqrt{r_k^2+\epsilon^2}-\epsilon)\right)}, \tag{53}$$

$$\frac{\partial g_r}{\partial w_{s,t}} = -\frac{1}{\overline{r}} \frac{\sum_{k=1}^{N_r} \frac{exp\left(-\tau(\sqrt{r_k^2+\epsilon^2}-\epsilon)\right) r_k \frac{\partial r_k}{\partial w_{s,t}}}{\sqrt{r_k^2+\epsilon^2}}}{\sum_{k=1}^{N_r} exp\left(-\tau(\sqrt{r_k^2+\epsilon^2}-\epsilon)\right)}, \tag{54}$$

where the gradient of the generic curvature radius can be evaluated thanking to Eq. (50). Details are provided in Appendix B.

5 Numerical Strategy

A suitable numerical strategy is described with the precise aim of solving the CNLPP formulated in Eq. (24). It is noteworthy that the proposed algorithm, excluding the postprocessing phase, has been developed in MATLAB: only the FEM analysis, which is needed for evaluating both objective and constraint functions, has been carried out by means of a commercial FE code (in this case ANSYS). This is a very important advantage because the proposed methodology is tested and interfaced with a widespread and widely customisable FEM software. Usually, the Method of Moving Asymptotes (MMA) is employed in TO [29]. Instead of the MMA, in this work the MATLAB *local optimization toolbox* and in particular the *active-set* algorithm of the *fmincon* family [30] with non linear constraints has been utilised to solve problem (24).

The active-set algorithm (ACS) is part of a special class of Sequential Quadratic Programming (SQP) algorithms for constrained optimisation problems which can tolerate some iterative steps out of the feasible region. This fact allows for an efficient exploration of the feasible domain (especially its boundary) in CNLPPs. The ACS method produces a sequence of sub-problems approximating the CNLPP at hand by exploiting the information provided by the gradient and by using only the violated constraints, which constitute, as a matter of fact, the âĂIJactive-setâĂİ. Then, these sub-problems are iteratively solved. Particularly, the ACS approximation is quadratic and the ACS algorithm is a quasi-Newton method that makes use of the Broyden-Fletcher-Goldfarb-Shanno (BFGS) formula to approximate the Hessian in order to save computational time, see [31]. The robustness and the efficiency of SQP methods in solving CNLPPs have been largely tested and they constitute a well-established class of gradient-based algorithms [31]. Moreover, SQP algorithms can be classified as "globally convergent" algorithms, in the sense that, provided a feasible starting point, the consequent solution found by the algorithm will always respect the optimality conditions for constrained optimisation, i.e. the so-called Karush-Kuhn-Tucker (KKT) conditions. Of course, the aforementioned features of SQP algorithms do not prevent from falling on a local optimum,

which is a common feature shared by all the other gradient-based algorithms (including MMA). Furthermore, the problem nature depends on the chosen objective and constraint functions, so nothing can be *a priori* stated about the convexity of the CNLPP at hand when these quantities are computed numerically through a FEM analysis. A deeper discussion on the convexity of TO problems, uniqueness of solution and dependence on initial data can be found in [2] and it is out of the scopes of this paper. A synthetic scheme of the proposed numerical strategy and its application to TO problems is shown in Fig. 1: inherent details concerning each block are given in the following.

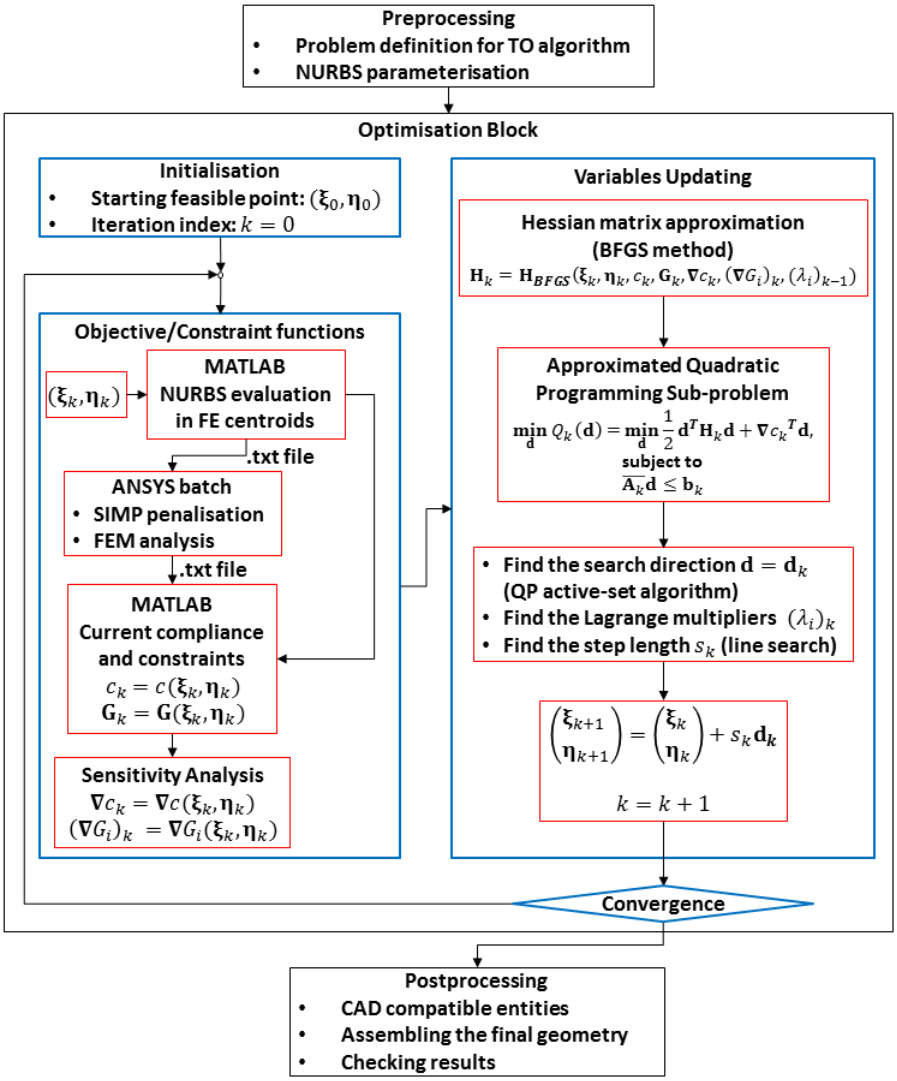

Figure 1: NURBS-based SIMP algorithm - synthetic scheme

- **Preprocessing** The design domain together with geometry, mesh, loads and boundary conditions for the structural problem at hand are established. Meanwhile, the NURBS is defined on the design domain in terms of number of control points $(n_u + 1)$ and $(n_v + 1)$ and blending functions degrees p and q. The objective function must be declared and the

optimisation constraints (if any) should be defined too. Furthermore, some Non-Design Regions (NDRs) or symmetry conditions can be set at this stage.

- **Optimisation block.** The generic CNLPP of compliance minimisation subject to m inequality constraints can be stated in the form

$$\begin{aligned} &\min_{\boldsymbol{\xi},\boldsymbol{\eta}} \ c(\boldsymbol{\xi},\boldsymbol{\eta}), \\ &\text{subject to:} \\ &G_i(\boldsymbol{\xi},\boldsymbol{\eta}) \leq 0, \ i = 1,...,m, \end{aligned} \tag{55}$$

where the FE equilibrium state equation has been neglected and all inequality constraints, including bounds on the design variables, are expressed in the compact form $\mathbf{G}(\boldsymbol{\xi},\boldsymbol{\eta}) \leq \mathbf{0}$. Classic SQP methods change the constrained optimisation problem into an unconstrained minimisation problem through a suitable Lagrangian function $L(\boldsymbol{\xi},\boldsymbol{\eta},\boldsymbol{\Lambda})$ defined as

$$L(\boldsymbol{\xi},\boldsymbol{\eta},\boldsymbol{\Lambda}) = c(\boldsymbol{\xi},\boldsymbol{\eta}) + \boldsymbol{\Lambda}^T \mathbf{G}(\boldsymbol{\xi},\boldsymbol{\eta}), \tag{56}$$

where $\boldsymbol{\Lambda}$ is a column vector constituted of m Lagrange multipliers, whose components must fulfil the following conditions

$$\begin{aligned} &\lambda_i = 0, \ if \ G_i(\boldsymbol{\xi},\boldsymbol{\eta}) \leq 0 \\ &\lambda_i > 0, \ if \ G_i(\boldsymbol{\xi},\boldsymbol{\eta}) > 0 \\ &\qquad \forall \ i = 1,...,m. \end{aligned} \tag{57}$$

A direct solution of problem (55) in terms of both design variables and Lagrange multipliers is not possible. Therefore, a sequence of quadratic approximations of the initial problem is generated and each problem is solved in an iterative loop.

Before proceeding with the algorithm description, it should be remarked that a suitable initialisation is needed. In particular, an initial guess for the design variables (NURBS control points and weights) is required for starting the solution search. According to the notation of Section 3, let $\boldsymbol{\xi_0}$ and $\boldsymbol{\eta_0}$ be the initial vectors of control points and weights respectively: suitable lower $\mathbf{lb}$ and upper $\mathbf{ub}$ bounds must be defined

$$\begin{cases} \mathbf{lb}_\xi \leq \boldsymbol{\xi_0} \leq \mathbf{ub}_\xi, \\ \mathbf{lb}_\eta \leq \boldsymbol{\eta_0} \leq \mathbf{ub}_\eta. \end{cases} \tag{58}$$

Moreover, some options for the ACS *fmincon* algorithm are set in this phase: the convergence tolerance on the objective function and on the design variables must be established. Moreover, a threshold on the maximum number of iterations is also introduced as a further stop criterion. The option on the gradient provision (sensitivity analysis formulae for both objective function and non-linear constraints) is activated here. Let $(\boldsymbol{\xi}_k,\boldsymbol{\eta}_k)$ be the values of design variables at iteration k: they are utilised in two main steps.

Firstly, the objective and constraints functions need to be calculated. To this aim, the NURBS representing the fictitious density is evaluated at the centroids of the elements and this information is transferred from MATLAB to ANSYS in a suitable format (which can be defined by the user). The SIMP criterion (13) is used to achieve the penalisation of mechanical properties and to perform the FEM analysis. Then, the required mechanical quantities are registered for each element and transferred to MATLAB. Now, it is possible to update the objective function (the compliance $c_k = c(\boldsymbol{\xi}_k, \boldsymbol{\eta}_k)$) and constraints ($\mathbf{G}_k = \mathbf{G}(\boldsymbol{\xi}_k, \boldsymbol{\eta}_k)$). Furthermore, thanks to the sensitivity analysis (refer to Section 3 and Section 4), the derivatives can be easily computed ($\nabla c_k, (\nabla G_i)_k, i = 1, ..., m$).

Secondly, the aforementioned quantities are used, together with the previous evaluation of Lagrange multipliers, to approximate the Hessian matrix according to the BFGS formula (refer to [30] and [31]). The approximated Hessian matrix $\mathbf{H}_k = \mathbf{H}_{BFGS}(\boldsymbol{\xi}_k, \boldsymbol{\eta}_k, c_k, (G_i)_k, \nabla c_k, (\nabla G_i)_k, (\lambda_i)_{k-1}),\ i = 1, ..., m$, is employed to state the active-set quadratic programming (QP) approximated problem, namely

$$\begin{aligned} \min_{\mathbf{d}} \ Q_k(\mathbf{d}) = \min_{\mathbf{d}} \ & \frac{1}{2}\mathbf{d}^T\mathbf{H}_k\mathbf{d} + \nabla c_k^T\mathbf{d}, \\ & \text{subject to:} \\ & \overline{\mathbf{A}}_k\mathbf{d} \leq \mathbf{b}_k, \end{aligned} \tag{59}$$

whose design variables are the search direction components collected in the vector $\mathbf{d}$. In Eq. (59), $\overline{\mathbf{A}}_k$ is the coefficient matrix, whilst $\mathbf{b}_k$ is a vector of constants, both given by the linearization employed by ACS algorithm for the optimisation constraints. The QP problem (59) can be solved taking advantage of one of the several methods in literature, see [31]. Hence, the current search direction ($\mathbf{d}_k$) is evaluated, together with the current value of Lagrange multipliers ($(\lambda_i)_k$). The last operation consists of finding a suitable step length (s_k) along the search direction $\mathbf{d_k}$. For a deeper insight into the matter, the reader is addressed to [31]. Finally, variables can be updated as follows:

$$\begin{aligned} \left\{ \begin{array}{c} \boldsymbol{\xi}_{k+1} \\ \boldsymbol{\eta}_{k+1} \end{array} \right\} &= \left\{ \begin{array}{c} \boldsymbol{\xi}_k \\ \boldsymbol{\eta}_k \end{array} \right\} + s_k\mathbf{d}_k, \\ k &= k + 1. \end{aligned} \tag{60}$$

Thus, the convergence criteria can be checked. The algorithm stops either if the maximum number of iterations is reached or if the predicted change of one among the following quantities is less than a suitable threshold value (10^{-6}):

- the objective function
- the gradient norm of the Lagrange function
- the vector of design variables.

Of course, the latter set of criteria makes sense only if the objective function and the imposed constraints are dimensionless.

- **Postprocessing.** The result of the optimisation is a fictitious density distribution on the reference domain represented through a NURBS scalar function. The outstanding advantage provided by the NURBS formulation stands on the possibility to export a CAD compatible entity in order to rebuild in a straightforward way the boundary of the optimised 2D structure. However, it is necessary to adapt the result to the NURBS formalism: in fact, a standard NURBS surface is implicitly defined by means of relations similar to Eq. (1). Indeed, each physical coordinate is function of the dimensionless parameters u and v. Thus, a full description of a NURBS surface is obtained through relations like $x = x(u, v)$, $y = y(u, v)$ and $z = z(u, v)$, where the respective coordinates of control points appear. Normally, the dimensionless parameters are not related to the physical coordinates x, y and z. Standard format files for NURBS data exchange (.igs) require control points coordinates in the three physical directions. However, in this discussion, we make use of a NURBS scalar function $\rho\,(u, v)$ wherein the physical coordinates x and y are related to u and v through Eqs. (21). Hence, it is not necessary to introduce x and y coordinates of control points during the optimisation but they must be provided in the postprocessing phase in order to set up the .igs file. Now, the z-coordinate of each control point is simply the value of the fictitious density for the considered control point (i.e. $\overline{\rho_{i,j}},\ i = 1, ..., n_u,\ j = 1, ..., n_v$) provided by the TO optimisation; x and y coordinates of control points should be chosen in such a way that the following conditions are met:

$$\begin{cases} x = \sum_{i=0}^{n_u} \sum_{j=0}^{n_v} R_{i,j}(u, v) \mathrm{P}_{\mathrm{x_{i,j}}}, \\ y = \sum_{i=0}^{n_u} \sum_{j=0}^{n_v} R_{i,j}(u, v) \mathrm{P}_{\mathrm{y_{i,j}}}. \end{cases} \tag{61}$$

The solution of problem (61) is known in literature and referred as Greville's abscissae [32], defined through the knot vectors and degrees, namely

$$\begin{cases} \mathrm{P}_{\mathrm{x_{i,j}}} = \dfrac{W}{p} \sum_{k=0}^{p} U_{i+k},\ \forall j = 1, ..., n_v, \\ \mathrm{P}_{\mathrm{y_{i,j}}} = \dfrac{H}{q} \sum_{k=0}^{q} V_{j+k},\ \forall i = 1, ..., n_u. \end{cases} \tag{62}$$

Once the computation is done, all the NURBS information are collected into an .igs file and the NURBS can be imported in a CAD software. Before proceeding, a threshold value for the density function is computed in MATLAB in such a way that optimisation constraints are met: a suitable plane placed at this density value can be cut by means of the NURBS surface in the CAD software in order to retrieve the final 2D boundaries of the optimised structure. Finally, a further .igs file is created with the final 2D geometry and it can be transferred to the FEM software for checking operations (i.e. in order to verify the value of both objective and constraint functions on the rebuilt structure). A summarizing scheme of the *Postprocessing* phase is depicted by Fig. 2.

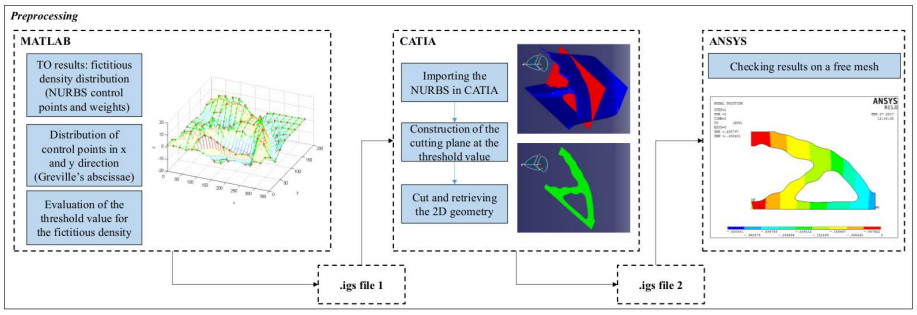

Figure 2: Postprocessing - synthetic scheme

6 Results and discussion

Some meaningful results are presented in this Section in order to prove the effectiveness of the proposed algorithm. The topologies of each optimised geometry is shown here on the final rebuilt structure after postprocessing phase. The CAD compatibility of NURBS is fully exploited, so useless elements have been easily cut off: therefore, the objective function and constraints are evaluated on the "true structure" instead of on the meshed reference domain (wherein "void" elements still hold on together with the "material" elements), that is meaningless from an engineering viewpoint. For each analysed test case, results are also compared with those provided by the commercial software OptiStruct [17] by using the same mesh of the reference domain. As stated in Section 3, two set of design variables, namely the NURBS control points and the weights, collected in the arrays $\boldsymbol{\xi}$ and $\boldsymbol{\eta}$ respectively (refer to Eqs. (22) and (23)), tune the topology of the 2D domain. For each case, the lower and upper bounds are fixed as follows:

- concerning the fictitious density at each control point, standard bounds are chosen, i.e. $lb_{\xi_{i,j}} = 10^{-3}$ and $ub_{\xi_{i,j}} = 1$, $\forall i = 0, ..., n_u$ and $\forall j = 0, ..., n_v$;
- weights enjoy greater freedom and it has been chosen $lb_{\eta_{i,j}} = 1/2$ and $ub_{\eta_{i,j}} = 10$, $\forall i = 0, ..., n_u$ and $\forall j = 0, ..., n_v$.

The first part of this section is dedicated to a comparison between the results obtained with NURBS and BSpline basis functions, respectively, on a standard benchmark. Then, more general examples are provided by imposing a specific material phase, namely "void" ($\rho = 0$) or "material" ($\rho = 1$) in some prescribed Non-Design Regions (NDRs) of the computational domain. Moreover, an application with a symmetry constraint is shown. Finally, the effects of the geometric constraints discussed in Section 4 are investigated.

6.1 Comparison between Bspline and NURBS surfaces for topology optimisation

The problem of the compliance minimisation with an imposed volume fraction is considered here for a standard benchmark: an aluminium cantilever plate. All geometric and material data are provided in the caption of Fig. 3. The aim of this first example is to compare the optimum topology

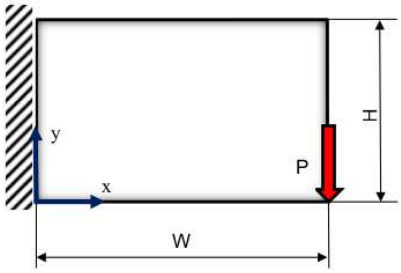

Figure 3: Cantilever plate problem - $W = 320\ mm$, $H = 200\ mm$, Thickness $t = 2\ mm$, Young Modulus $E = 72000MPa$, Poisson Modulus $\nu = 0.33$, Load $P = 1000\ N$.

of the domain resulting from the utilisation of Bspline and NURBS surfaces, respectively. When using the Bspline surface the TO problem can be stated as

$$\begin{aligned} &\min_{\boldsymbol{\xi}} \ \ c(\rho(\boldsymbol{\xi})), \\ &\text{subject to:} \\ &\begin{cases} [\mathrm{K}]\{\mathrm{U}_{FEM}\} = \{\mathrm{F}\}, \\ \dfrac{V(\rho_e)}{V_{tot}} = 0.4, \\ \mathbf{lb}_\xi \leq \boldsymbol{\xi} \leq \mathbf{ub}_\xi, \end{cases} \end{aligned} \tag{63}$$

thus all the weights get the same value and can be excluded from the design space. Conversely, when using the more general NURBS formalism, the TO problem is

$$\begin{aligned} &\min_{\boldsymbol{\xi},\boldsymbol{\eta}} \ \ c(\rho(\boldsymbol{\xi},\boldsymbol{\eta})), \\ &\text{subject to:} \\ &\begin{cases} [\mathrm{K}]\{\mathrm{U}_{FEM}\} = \{\mathrm{F}\}, \\ \dfrac{V(\rho_e)}{V_{tot}} = 0.4, \\ \mathbf{lb}_\xi \leq \boldsymbol{\xi} \leq \mathbf{ub}_\xi, \\ \mathbf{lb}_\eta \leq \boldsymbol{\eta} \leq \mathbf{ub}_\eta. \end{cases} \end{aligned} \tag{64}$$

Both problems (63) and (64) have been solved through the procedure described in Section 5 for three values of surface degrees , i.e. $p, q = 2, 3, 4$, and three different values of the overall number of control points, i.e. $(n_u + 1) \times (n_v + 1) = 16 \times 10,\ 32 \times 20,\ 48 \times 30$. The FE model of the rectangular domain is discretised by means of Ansys SHELL181 elements, i.e. shell elements with 4 nodes and 6 DOFs per node [33]. After a preliminary check on the convergence of the results, the size of the *mapped* mesh of the rectangular domain has been chosen equal to 80×50 elements. The equality constraint is split in two inequality constraints by considering a tolerance of 0.005 on the value of f. Then, the volume fraction constraint will be met if $0.395 < \dfrac{V(\rho_e)}{V_{tot}} < 0.405$. Results are provided in terms of compliance c and volume fraction V/V_{tot} of the final optimum topologies in captions of Figs. 4-9.

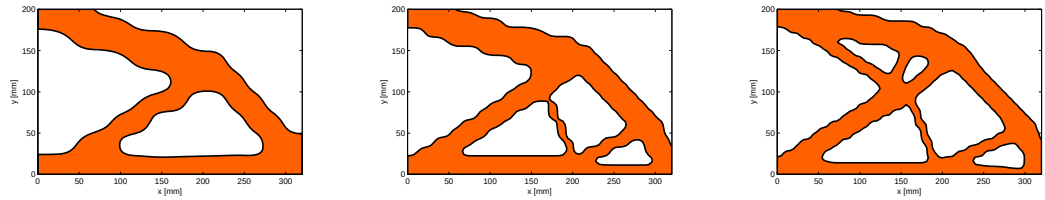

(a) $(n_u + 1) \times (n_v + 1) = 16 \times 10$, $c = 426.31\ Nmm$, $V/V_{tot} = 0.4003$.

(b) $(n_u + 1) \times (n_v + 1) = 32 \times 20$, $c = 400.63\ Nmm$, $V/V_{tot} = 0.4134$.

(c) $(n_u + 1) \times (n_v + 1) = 48 \times 30$, $c = 403.45\ Nmm$, $V/V_{tot} = 0.4020$.

Figure 4: BSpline results for $p, q = 2$

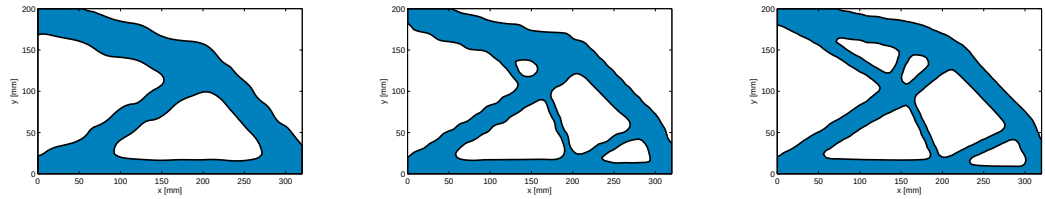

(a) $(n_u + 1) \times (n_v + 1) = 16 \times 10$, $c = 413.96\ Nmm$, $V/V_{tot} = 0.4042$.

(b) $(n_u + 1) \times (n_v + 1) = 32 \times 20$, $c = 403.49\ Nmm$, $V/V_{tot} = 0.4044$.

(c) $(n_u + 1) \times (n_v + 1) = 48 \times 30$, $c = 394.81\ Nmm$, $V/V_{tot} = 0.4036$.

Figure 5: NURBS results for $p, q = 2$

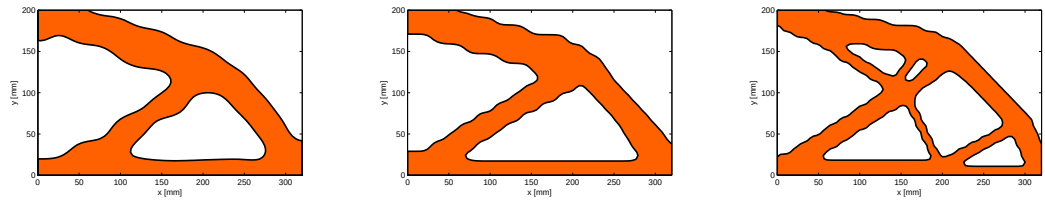

(a) $(n_u + 1) \times (n_v + 1) = 16 \times 10$, $c = 432.29\ Nmm$, $V/V_{tot} = 0.4011$.

(b) $(n_u + 1) \times (n_v + 1) = 32 \times 20$, $c = 408.37\ Nmm$, $V/V_{tot} = 0.3994$.

(c) $(n_u + 1) \times (n_v + 1) = 48 \times 30$, $c = 402.39\ Nmm$, $V/V_{tot} = 0.4025$.

Figure 6: BSpline results for $p, q = 3$

Furthermore, numerical results concerning the true compliance as function of the number of control points are synthetically plotted in Fig. 10. It is interesting to compare this compliance with the compliance calculated on the reference domain at the end of the solution phase before the cutting operation, i.e. the compliance of the whole rectangular domain constituted by all elements with the respective pseudo-density value (it is referred as “projected compliance", see Fig. 11).

The following remarks arise from the analysis of the numerical results:

a) Topologies obtained through a NURBS-based representation of the fictitious density function are smoother than those obtained by means of BSpline-based description, see Figs. 4-9. Moreover, as clearly shown in Fig. 11, the optimum topology obtained using NURBS surfaces

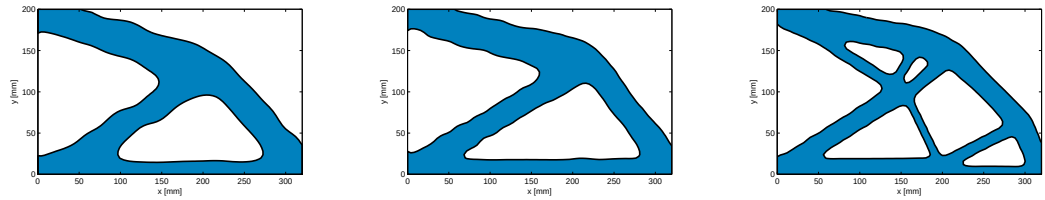

(a) $(n_u + 1) \times (n_v + 1) = 16 \times 10$, $c = 416.96\ Nmm$, $V/V_{tot} = 0.4048$.

(b) $(n_u + 1) \times (n_v + 1) = 32 \times 20$, $c = 404.07\ Nmm$, $V/V_{tot} = 0.4050$.

(c) $(n_u + 1) \times (n_v + 1) = 48 \times 30$, $c = 394.45\ Nmm$, $V/V_{tot} = 0.4047$.

Figure 7: NURBS results for $p, q = 3$

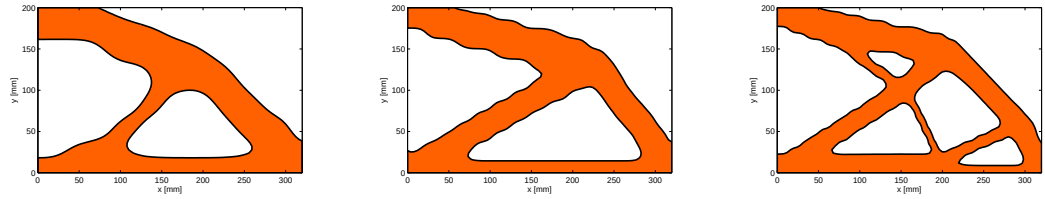

(a) $(n_u + 1) \times (n_v + 1) = 16 \times 10$, $c = 446.71\ Nmm$, $V/V_{tot} = 0.4020$.

(b) $(n_u + 1) \times (n_v + 1) = 32 \times 20$, $c = 407.31\ Nmm$, $V/V_{tot} = 0.4032$.

(c) $(n_u + 1) \times (n_v + 1) = 48 \times 30$, $c = 401.69\ Nmm$, $V/V_{tot} = 0.4009$.

Figure 8: BSpline results for $p, q = 4$

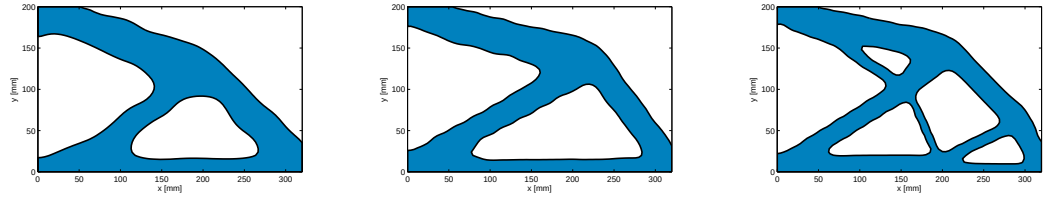

(a) $(n_u + 1) \times (n_v + 1) = 16 \times 10$, $c = 433.01\ Nmm$, $V/V_{tot} = 0.4039$.

(b) $(n_u + 1) \times (n_v + 1) = 32 \times 20$, $c = 409.09\ Nmm$, $V/V_{tot} = 0.4044$.

(c) $(n_u + 1) \times (n_v + 1) = 48 \times 30$, $c = 403.12\ Nmm$, $V/V_{tot} = 0.4047$.

Figure 9: NURBS results for $p, q = 4$

takes lower values of the projected compliance when compared to those resulting from a BSpline-based representation. This fact justifies the utilisation of the more general NURBS surfaces formalism. However, when looking at the true compliance (Fig. 10), NURBS have still significantly better performances than the respective BSplines only when the number of control points is kept small. If the number of control points increases, even if NURBS topologies are still smoother than BSpline topologies, the decrease of the objective function disappears and, sometimes, a BSpline solution could be better than a NURBS solution (refer to the cases of Fig. 8b and Fig. 9b). Thus, the utilisation of NURBS instead of BSpline surfaces in TO must be carefully assessed.

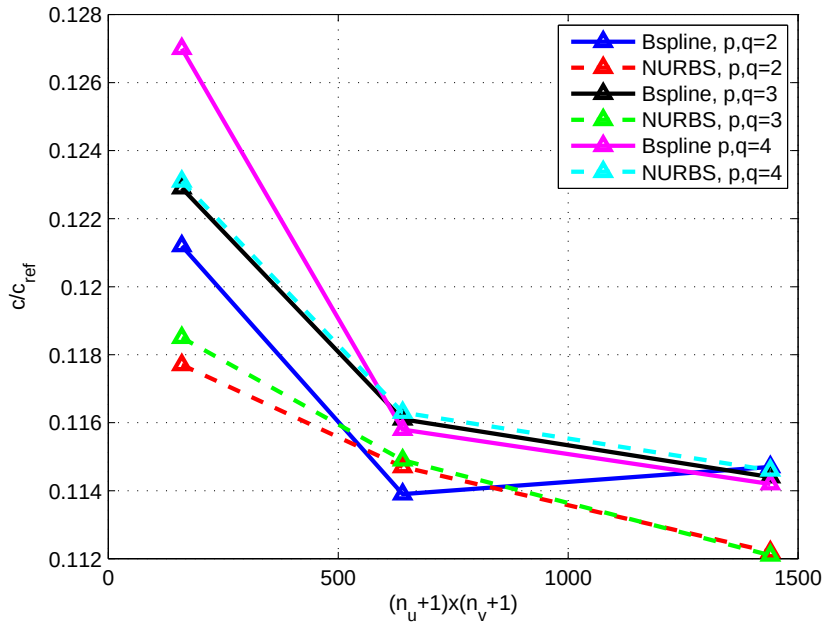

Figure 10: Cantilever plate problem - True compliance trends.

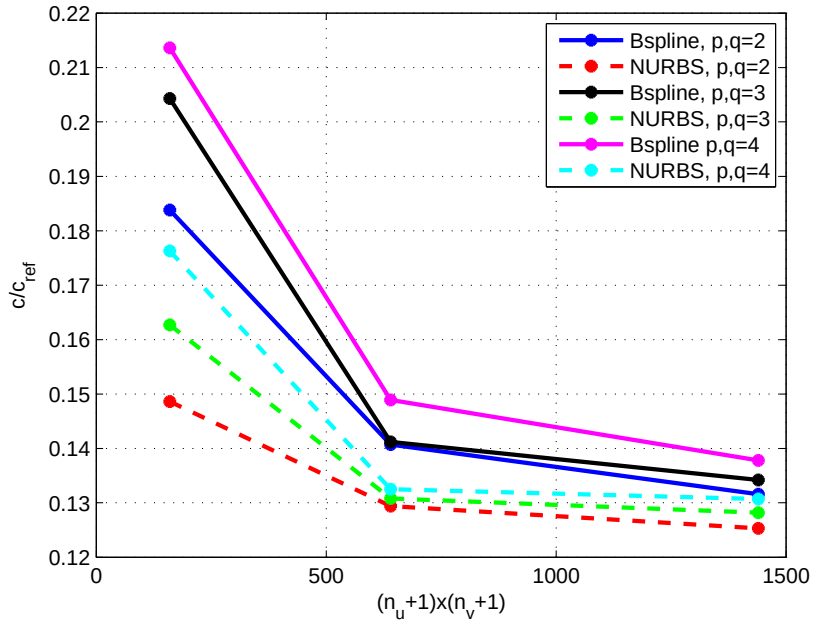

Figure 11: Cantilever plate problem - Projected compliance trends.

b) Taking inspiration from [16], the behaviour of the solutions has been investigated by varying both the number of control points $(n_u + 1) \times (n_v + 1)$ and the degrees of the surface (p, q). These parameters affect the dimension of the local support of the blending functions. The local support, in the context of TO, behaves as a *filter zone*, i.e. a region of the reference domain wherein the densities of "neighbour elements" are interdependent. Such a filter

zone is sought in standard density-based algorithms to prevent the checker-board effect [2]. Therefore, the NURBS-based SIMP method naturally ensures an implicitly-defined filter zone without the need of introducing artificial distance-based filters as in [2]. This aspect is strictly related to the *local support property* of NURBS blending functions [25]: the filter dimensions increase if the degrees increase or if the number of control points decreases. Conversely, as the degrees decrease and the number of control points increases, the filter get smaller. Taking into account these considerations, it seems natural that thinner topology elements (branches) are allowed when the dimensions of the filter zone decrease. This trend is evident in BSpline and NURBS benchmarks, see Figs. 4-9: BSpline and NURBS surfaces sharing the same degrees, knot-vectors components and same control point coordinates have the same filter zone. Furthermore, the smaller is the filter size, the lower is the true compliance value.

c) Several remarks arise from a deeper investigation of results shown in Fig. 10 and Fig. 11. Firstly, the projected compliance trend is smoother than the respective true compliance trend. This fact is a consequence of the cut operation in the postprocessing phase, which constitutes a a sort of “discontinuity" from a mathematical viewpoint. Indeed, this cutting operation can lead to a pseudo-optimum solution: the objective function decreases but constraints are not met (see for example the solution of Fig. 4b). Secondly, the projected compliance exhibits an early phase of a plateau (Fig. 11), that disappears in the graph of the true compliance of Fig. 10. Actually, considering the decrease of the objective function as the number of control points increases, it can be stated that the true compliance does not depend any more on the number of control points beyond a certain threshold value. In other words, increasing the number of design variables beyond a certain threshold value does not imply better performances, even if the topology could appear different (see sub-figures b and c of Figs. 4-9). This result allows for introducing a sort of “design rule": the number of control points (design variables) can be chosen and tuned as a compromise between accuracy in the topology description and time saving in running the algorithm.

d) It is noteworthy that the projected compliance is always greater than the respective true compliance: this point is of paramount importance because it means that the NURBS-based SIMP approach is conservative.

Finally, results are compared to those obtained from Hyperworks OptiStruct, where the TO problem of Fig. 3 is solved on the same reference domain meshed through 80×50 PSHELL Elements [17]. Of course, being the software founded on a classic density-based method, the design variables are the element densities. Moreover, the final rebuilt optimum topology is obtained by means of a smoothing phase (OSSmooth module of Altair Hyperworks package). It is pointed out that OptiStruct needs a minimum member size constraint to properly work: in fact, the minimum member size acts as a filter for TO. In this case, a minimum member size $d_{min} = 12\ mm$ has been chosen (i.e. 3 times the mesh size, as suggested by OptiStruct's reference guide).

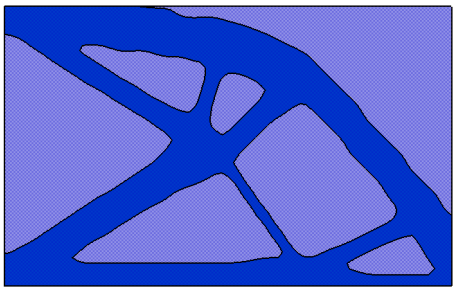

Figure 12: Hyperworks-OptiStruct solution of the cantilever plate problem: $c = 398.66\ Nmm$, $V/V_{tot} = 0.3992$.

Let us consider the BSpline-based solution of Fig. 6c and the NURBS-based solution of Fig. 7c with $p = q = 3$ and $(n_u + 1) \times (n_v + 1) = 48 \times 30$. Both the topologies, as well as the OptiStruct solution, meet the volume constraint. As far as the true compliance is concerned, for the OptiStruct solution it is obtained $c = 398.66\ Nmm$ (4000 design variables), for the BSpline-based solution $c = 402.39\ Nmm$ (1440 design variables) and for the NURBS-based solution $c = 394.45\ Nmm$ (2880 design variables). Consequently, it can be stated that the NURBS-based algorithm and the software OptiStruct provide consistent results. Finally, it can be asserted that in the framework of the NURBS-based SIMP approach the optimum topology (showing equal or superior performances when compared to those provided by the classical SIMP approach) is obtained with a considerable reduction in the number of design variables.

6.2 Influence of Non-Design Regions

In order to show the versatility of the proposed method, the effects of two prescribed NDRs are investigated in this Section. The problem of Fig. 3 has been slightly changed, as it is shown in Fig. 13: a circular sector (red zone in which $\rho = 1$, centred at $x = W/2$, $y = H/2$ with $R_{int} = 40$mm, $R_{ext} = 50$mm) surrounding a "void" circle (yellow zone wherein $\rho = 0$) has been defined over the rectangular plate.

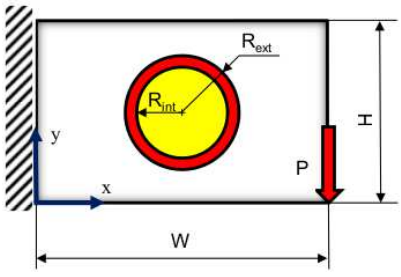

Figure 13: Cantilever plate problem with NDRs: design domain in white, prescribed material NDR in red, prescribed void NDR in yellow.

In this case, a BSpline surface is utilised to get the solution, its parameters are $p = q = 3$ and $(n_u + 1) \times (n_v + 1) = 48 \times 30$.

The optimum solutions provided by both the NURBS-based SIMP approach and the classic

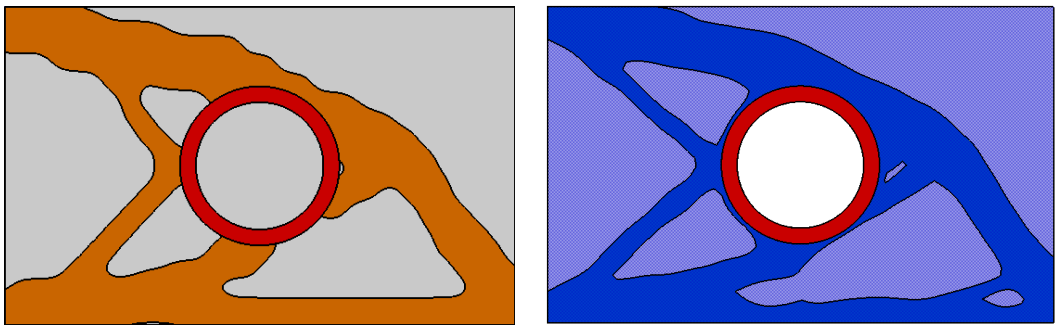

(a) NURBS-based SIMP solution, $c = 425.95\ Nmm$, $V/V_{tot} = 0.3997$.

(b) Hyperworks-OptiStruct solution, $c = 406.37\ Nmm$, $V/V_{tot} = 0.4085$.

Figure 14: Cantilever plate problem with NDRs.

SIMP method are illustrated in Fig. 14 (the values of the true compliance and of the constraint on the volume fraction are reported in the figure captions). As it can be easily noticed, the percentage difference in terms of the objective function is lower than 5%, while the overall volume fraction provided by the NURBS-based SIMP approach is lower than that resulting from the classic SIMP approach: in the latter case, the constraint on the volume fraction is not met. Therefore, these solutions (which are slightly different in terms of topological branches) are "equivalent" and consistent from an engineering viewpoint with a considerable difference: in this case the fictitious density field represented through a NURBS surface is characterised "only" by 1440 design variables while the OptiStruct model is characterised by 2392 design variables.

6.3 Influence of a symmetry constraint

In this Section, the problem shown in Fig. 3 and described by Eqs. (63) and (64) is enhanced with a further geometric constraint: the topology is forced to be symmetric with respect to the plane $y = H/2$. In this case the BSpline and NURBS main parameters are set as follows: $p = q = 3$ and $(n_u + 1) \times (n_v + 1) = 48 \times 30$. The numerical values of compliance and volume fraction are collected in captions of Fig. 15a and Fig. 15b.

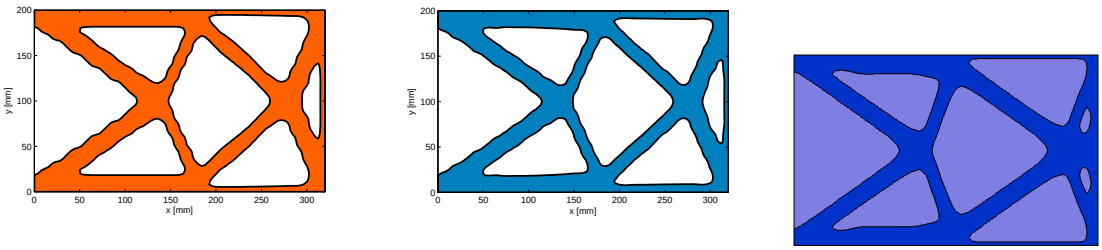

(a) BSpline solution: $c = 454.80\ Nmm$, $V/V_{tot} = 0.4010$.

(b) NURBS solution: $c = 456.47\ Nmm$, $V/V_{tot} = 0.4044$.

(c) Hyperworks-OptiStruct solution, $c = 443.87\ Nmm$, $V/V_{tot} = 0.4036$.

Figure 15: Cantilever plate problem with symmetry constraint

The same problem has been solved in OptiStruct environment and results are depicted in Fig.

15c. The symmetry constraint allows for halving the number of variables, so the BSpline solution is characterised by a compliance $c = 454.80\ Nmm$ with 720 design variables, the NURBS one by a compliance $c = 456.47\ Nmm$ with 1440 design variables, whilst for the OptiStruct solution it is obtained $c = 443.87\ Nmm$ with 2000 design variables.

6.4 Minimum member size

In this example, problem (63) is solved for the benchmark illustrated in Fig. 3 by considering the minimum member size constraint of Eq. (31). Particularly, the TO problem is solved by means of a BSpline surface with $(n_u+1)\times(n_v+1) = 48\times30$ control points and $p = q = 3$. The constraint on the minimum member size is imposed by considering three values of d_{min}, i.e. 16, 20, and 25 mm. Results are collected in Figs. 16-18 for each analysis. In each figure, the first image is the rebuilt geometry provided by the NURBS-based SIMP method after the postprocessing phase, whilst the second image is the final rebuilt geometry provided by the commercial tool OptiStruct. The FE model of the reference domain is the same as that illustrated in Sub-Section 6.1.

Two remarks of paramount importance can be inferred from the analysis of the results depicted in Figs. 16-18:

- All the advantages related to the NURBS geometrical properties are fully exploited in this case. Thanks to the combined action of the local support property and of the minimum member size constraint, all the meaningless "grey" zones are filtered and the final topology exactly meets the minimum member size constraint. Conversely, even if the optimum topologies resulting from OptiStruct are characterised by better performances in terms of the compliance value, they systematically do not meet the minimum member size constraint due to the presence of thin topological branches. Quantitatively, the minimum size provided by OptiStruct is 8 mm instead of 16 mm for the first case, 8 mm instead of 20 mm for the second one and 7 mm instead of 25 mm for the last one.

- The optimum solutions provided by the NURBS-based SIMP approach show non smooth boundaries. Indeed this aspect is related to the formulation of the minimum member size constraint according to the Poulsen's formula, see Eq. (31). As discussed in [19] the minimum member size is evaluated, for each element, only along four directions (see Section 4.1) in order to reduce the computational effort. Therefore, smoother boundaries can be got by increasing the number of checking direction in the Poulsen's equation.

6.5 Maximum member size

In order to show the effectiveness of the maximum member size in the framework of the NURBS-based SIMP approach, a suitable benchmark is proposed herein. As illustrated in Fig. 19, in this case a rectangular domain subject to a traction load is considered. All the material and geometrical

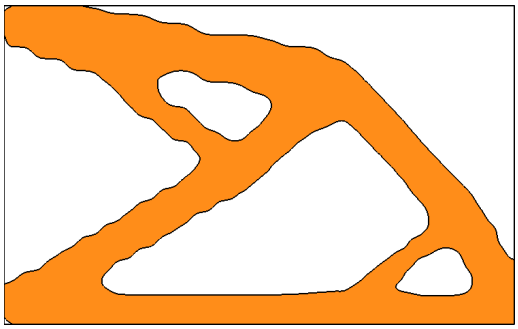

(a) BSpline solution: $c = 441.98\ Nmm$, $V/V_{tot} = 0.3996$.

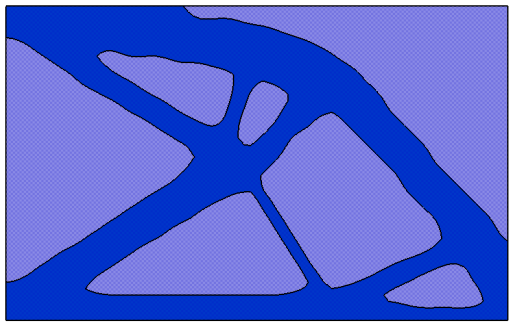

(b) Hyperworks-OptiStruct solution: $c = 401.02\ Nmm$, $V/V_{tot} = 0.3994$.

Figure 16: Results of the cantilever plate problem for $d_{min} = 16\ mm$

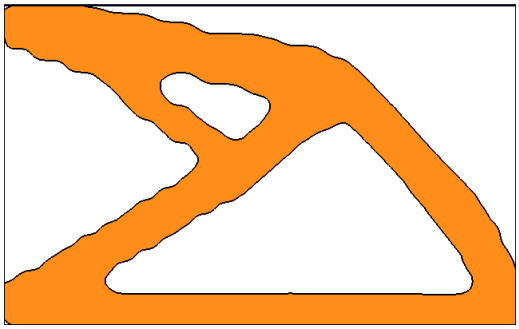

(a) BSpline solution: $c = 438.78\ Nmm$, $V/V_{tot} = 0.4027$.

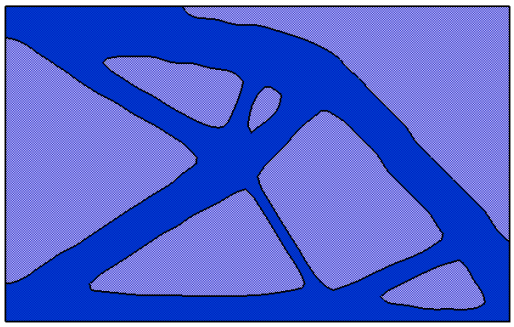

(b) Hyperworks-OptiStruct solution: $c = 400.22\ Nmm$, $V/V_{tot} = 0.0.4006$.

Figure 17: Results for $d_{min} = 20\ mm$

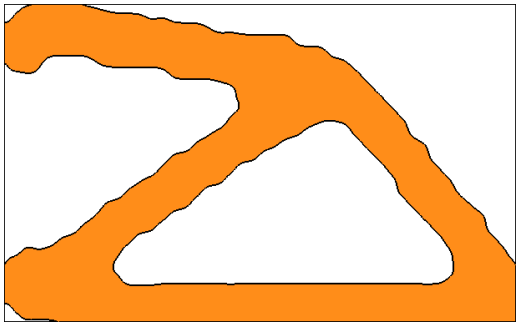

(a) BSpline solution: $c = 488.57\ Nmm$, $V/V_{tot} = 0.4036$.

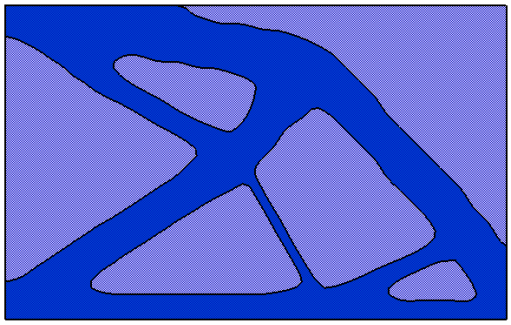

(b) Hyperworks-OptiStruct solution: $c = 400.73\ Nmm$, $V/V_{tot} = 0.4000$.

Figure 18: Results for $d_{min} = 25\ mm$

data are provided in the caption of Fig. 19. After a preliminary check on the convergence of the results, the rectangular domain is discretised by means of 100×50 shell elements.

A BSpline surface ($p = q = 3$, $(n_u + 1) \times (n_v + 1) = 40 \times 20$) is chosen to perform the TO analysis. Firstly, a standard problem similar to Eq. (63) is solved (the only modification is the

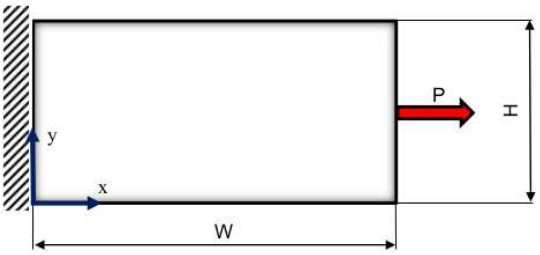

Figure 19: Traction plate problem - $W = 400\ mm$, $H = 200\ mm$, Thickness $t = 2\ mm$, Young Modulus $E = 72000 MPa$, Poisson Modulus $\nu = 0.33$, Load $P = 1000\ N$.

volume fraction equality constraint that becomes an inequality constraint):

$$\begin{aligned} &\min_{\boldsymbol{\xi}} \ \ c(\rho(\boldsymbol{\xi})), \\ &\text{subject to:} \\ &\begin{cases} [\mathrm{K}]\{\mathrm{U}_{FEM}\} = \{\mathrm{F}\}, \\ \dfrac{V(\rho_e)}{V_{tot}} - 0.4 \leq 0, \\ \mathbf{lb}_\xi \leq \boldsymbol{\xi} \leq \mathbf{ub}_\xi. \end{cases} \end{aligned} \tag{65}$$

Then, the introduction of a maximum member size constraint is investigated: in particular, the maximum allowable dimension of topological elements is fixed to $d_{max} = 25\ mm$. The maximum member constraint has been formulated according to Eq. (45) and the new problem to be solved is:

$$\begin{aligned} &\min_{\boldsymbol{\xi}} \ \ c(\rho(\boldsymbol{\xi})), \\ &\text{subject to:} \\ &\begin{cases} [\mathrm{K}]\{\mathrm{U}_{FEM}\} = \{\mathrm{F}\}, \\ \dfrac{V(\rho_e)}{V_{tot}} - 0.4 \leq 0, \\ g_{d_{max}} \leq 0, \\ \mathbf{lb}_\xi \leq \boldsymbol{\xi} \leq \mathbf{ub}_\xi. \end{cases} \end{aligned} \tag{66}$$

Solutions of problems (65) and (66), provided by both the proposed approach and OptiStruct are shown in Figs. 20a and 20b, respectively.

Concerning the optimum topology solution of problem (65), it can be stated that the NURBS-based SIMP method provides consistent results with those obtained by means of the commercial software OptiStruct from a numerical point of view: the percentage difference is 3.7%, but the number of design variables for the NURBS-based SIMP approach is significantly smaller (800) than that characterising the OptiStruct solution (5000). When considering problem (66), the percentage difference among the NURBS-based solution and the OptiStruct solution reduces to 2.1%. However, in the second case, significant topology changes can be observed, see Fig. 20b and Fig. 21b. Moreover, it should be pointed out that the maximum member size constraint, as well as the minimum member size constraint, has been formulated in *global sense* and not in *local sense*: this means that, even if the constraint of Eq. (45) is globally met during the iterations (on the

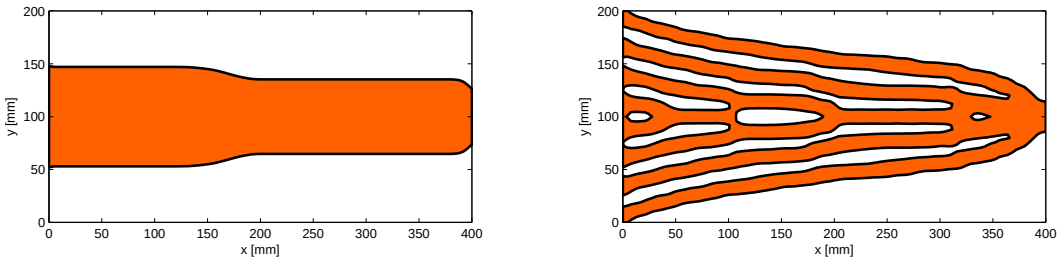

(a) $c = 55.85\ Nmm$, $V/V_{tot} = 0.4000$.

(b) $d_{max} = 25\ mm$, $c = 74.47\ Nmm$, $V/V_{tot} = 0.3984$.

Figure 20: NURBS-based SIMP solutions for the traction plate problem (a) without and (b) with maximum member size constraint.

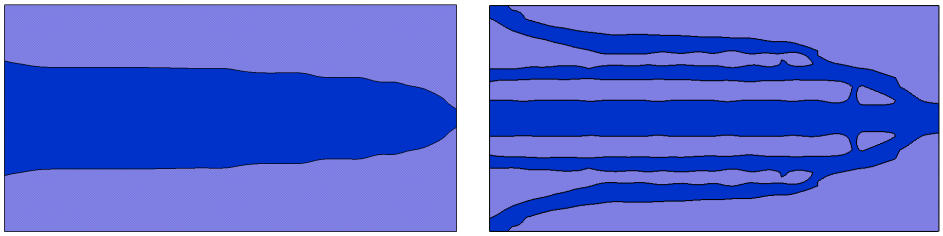

(a) $c = 58.02\ Nmm$, $V/V_{tot} = 0.3938$.

(b) $c = 72.95\ Nmm$, $V/V_{tot} = 0.3832$, $d_{max} = 25\ mm$.

Figure 21: Hyperworks-OptiStruct solution of the traction plate problem (a) without and (b) with maximum member size constraint.

meshed reference domain), it will not be necessarily satisfied locally after the postprocessing phase (i.e. when the geometry is rebuilt in order to be CAD-compatible). In other words, if the size of topological elements is measured on the rebuilt geometry, the maximum member size of 25 mm is not necessarily met in the proximity of the region where the load is applied, see Figs. 20b and 21b. Nevertheless, this circumstance is more critical as far as concerns the solution provided by OptiStruct. In particular, the OptiStruct solution shows a central branch of approximately 30 $mm > 25\ mm$ (see Fig. 21b), thus the constraint is violated on a larger portion of the definition domain when compared to the NURBS-based SIMP algorithm solution.

6.6 Local Curvature Radius

The constraint on the local curvature radius is tested here. Problem (63) is taken as reference and the constraint of Eq. (52) is considered. In particular, a minimum curvature radius $\overline{r} = 7.5\ mm$ is imposed. In this Section, the solution of Fig. 6b is taken as a reference solution, i.e. the constraint on the local radius of curvature is not imposed. For sake of completeness, it is recalled that the considered topology has been obtained through a BSpline surface ($p = q = 3$, $(n_u + 1) \times (n_v + 1) =$

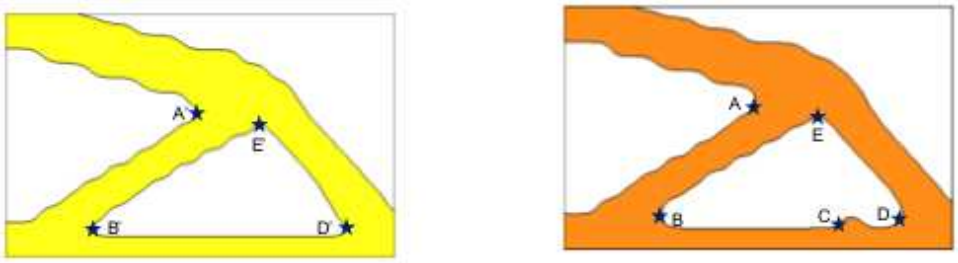

(a) $c = 408.37\ Nmm$, $V/V_{tot} = 0.3994$.

(b) $c = 412.00\ Nmm$, $V/V_{tot} = 0.3997$, $r_{min} = 10\ mm$.

Figure 22: Solution of the cantilever plate problem (a) without and (b) with the minimum local curvature radius constraint

32×20). Critical curvature points are highlighted in Fig. 22a and the respective curvature radii are: $r_{A'} = 4.4\ mm\ r_{B'} = 2.7\ mm$, $r_{D'} = 4.4\ mm$, $r_{E'} = 4.7\ mm$. The solution of the same problem enhanced with the minimum curvature radius constraint is illustrated in Fig. 22b. The critical curvature radii are: $r_A = 9.3\ mm$, $r_B = 8.9\ mm$, $r_C = 8.7\ mm$, $r_D = 8.9\ mm$, $r_E = 7.8\ mm$.

This last example allows for understanding the true potential hidden behind the NURSB-based SIMP approach. The NURBS formulation permits to have a precise and well-defined geometric description of the boundary of the topology at each iteration during the solution process, thus local quantities (like the curvature radius) can be easily computed by means of the NURBS formalism. Furthermore, in this last case a comparison with the results provided by OptiStruct is no longer possible simply because this feature cannot be realised in the framework of the classical SIMP approach.

7 Conclusions and Perspectives

This paper introduces and discusses a new formulation of the popular SIMP TO method in the NURBS mathematical framework. The effectiveness of the proposed approach is proven through some meaningful benchmarks which take into account for equality and/or inequality constraints. The well-known minimum and maximum member size constraints have been reformulated according to the NURBS formalism and a new constraint on the local curvature radius has been implemented. A suitable sensitivity analysis has been carried out for the objective function and for each constraint.

The proposed NURBS-based SIMP approach constitutes a generalisation of Qian's work [16]: in the proposed algorithm, the fictitious density function is represented by means of NURBS surfaces instead of simple BSpline functions. Qian's considerations on the effects of standard NURBS parameters on the obtained topologies are confirmed in this paper: the NURBS degrees and the number of control points have a direct impact on the dimensions of the local support of the NURBS blending functions, which acts as a filter in TO. In particular, the smaller is the filter, the thinner

are the members dimensions and better performances (a lower value of objective function) can be obtained.

The present work goes beyond the results of Qian's work because of the following reasons:

- the NURBS-based SIMP method allows for obtaining equivalent (or superior) performances with a reduced number of design variables (i.e. the density at each control point and the related weight) when compared to the classical SIMP approach wherein the optimisation variables are the element densities;
- the advantages of NURBS are fully exploited in terms of their CAD compatibility: a suitable postprocessing phase can be implemented and utilised in order to straightforwardly obtain the final optimised geometry for the problem at hand;
- when looking at the resulting topologies and the trend of the true compliance, it can be inferred that increasing the number of design variable beyond a certain threshold value does not imply an improvement of the objective function, thus the number of control points should be chosen as compromise between geometric accuracy and computational burden;
- a further fine point of the NURBS-based algorithm concerns the objective function check after the postprocessing phase. It has been verified that the true compliance, evaluated on the rebuilt structure after the postprocessing phase, is always lower than the projected compliance (i.e. the one of the reference domain with all mesh elements). In this sense, the proposed method is conservative;
- the insertion of the NURBS weights among the design variables deserves a special attention. When the fictitious density distribution is expressed by means of a NURBS surface, the boundaries of the optimum topology (after the postprocessing phase) are smoother than those observed when using a BSpline surface. This is due to the presence of weights which allow for reducing (or avoiding) the undesired "wave effect". However, it has been verified that a NURBS solution is not necessarily better than the respective BSpline solution in terms of true compliance. Since using a NURBS instead of a BSpline implies doubling the number of design variables, it is suggested, when dealing with a new TO problem, to launch a first TO analysis by using a Bspline representation of the pseudo-density function and to consider a NURBS surface only if the optimum topology has not a smooth boundary;
- the robustness of the NURBS-based SIMP method has been tested through the integration of Non-Design Regions and symmetry constraints;
- classical geometric constraints like minimum and maximum member size are reformulated using NURBS formalism and the derivatives with respect to control points densities and weights have been computed in a closed form. The robustness as well as the effectiveness of the proposed NURBS-based SIMP approach is also proven by dealing with benchmarks involving this kind of local features. Thanks to a special geometrical property of the NURBS

blending functions, i.e. the well-known *local support property*, an implicit filter zone (whose size depends upon the NURBS parameters) is always defined during the iterations (without the need of introducing numerical artefacts). Accordingly, on the one hand the undesired checker-board effect is always prevented, while on the other hand minimum and maximum admissible size are always globally met (before postprocessing phase) and almost always locally satisfied after rebuilding the optimum geometry. These considerations do not apply for the optimum topologies resulting from the classical SIMP algorithm;

- a new geometric constraint on the local curvature radius has been implemented. In the framework of the NURBS formalism this is a relatively straightforward task because a well-defined geometric description of the boundary of the current topology is always available during the iterations. To the best of the authors' knowledge this kind of features is not available for the classical SIMP algorithm.

Future perspectives are manifold and deal with several aspects of Topology Optimisation.

a) The development of a suitable tool to manage the solutions provided by the NURBS-based algorithm is forecast. Currently, the postprocessing phase relies on the utilisation of CAD commercial software (e.g. CATIA), so a more specific and dedicated tool is necessary in order to facilitate the control points displacement or weights arrangement by an external user which could not be familiar with TO concepts. Being the density function available in the form of NURBS/BSpline surfaces, some smoothing tool can be integrated in the method in order to smooth the BSpline "wave effect" or the indented boundary occurring when Poulsen's formulation of the minimum member size constraint is utilised.

b) The encouraging results obtained for 2D structures advise to extend the NURBS-based SIMP approach to the more general case of 3D problems. In this case, the fictitious density function would be related to a four-dimension hyper-surface and its intersection with a suitable hyperplane (threshold value) would provide the boundary of the solid. Research is ongoing on this aspect.

c) The library of possible optimisation responses (objective/constraint functions) should be extended: in order to effectively design/optimise real-world engineering structures under operative service conditions, suitable constraints should be implemented. These constraints could include purely mechanical features (e.g. plasticity and failure criteria, buckling, eigen-frequencies, etc.) or specific requirements (e.g. imposed displacements/rotations in some prescribed regions). Nevertheless, multiphysics studies are possible in the context of the NURBS-based TO algorithm, so other kind of physical quantities, like temperature or heat flow, can be taken into account.

d) Recent progresses in metal Additive Manufacturing (AM) make this technology extremely interesting for manufacturing the topologies provided by the optimisation process. Integrating AM constraints in the NURBS-based SIMP approach (through a dedicated formulation),

as support material limitation or other kinds of customisable cost functions, constitutes an important challenge for the following of this study.

e) The numerical results are extremely encouraging and, among the future perspectives, it could be possible to include, within the NURBS-based TO approach, the most relevant features related to the problem of the multiscale TO of structures. In this background, an interesting real-world engineering application could deal with the problem of designing *lattice* structures. This class of structures has gained an increasing attention since lattices can be easily manufactured by means of AM processes. Currently, they are utilised in several fields: scaffolds for prosthesis (biomedical field), crashworthiness parts (automotive and aerospace fields), etc. Of course, in this context, a suitable homogenisation technique should be coupled to the present NURBS-based TO algorithm.

acknowledgements

The first author is grateful to the Nouvelle-Aquitaine region for its contribution to this paper through the FUTURPROD project.

Appendix A : Sensitivity Analysis of Compliance and Volume Fraction

Let G be a generic scalar quantity whose gradient with respect to the mesh elements is known (i.e. $\frac{\partial G}{\partial \rho_e}$). Now, the derivatives $\frac{\partial G}{\partial \overline{\rho_{s,t}}}$ and $\frac{\partial G}{\partial w_{s,t}}$ need to be computed, where $\overline{\rho_{s,t}}$ is the generic control point of the NURBS scalar function and $w_{s,t}$ the respective weight. Let $I_{s,t}$ be the local support of the blending function associated to the control point $\overline{\rho_{s,t}}$: it is evident that only those elements lying in the support will contribute to the sensitivity analysis. Therefore, the following general expressions can be inferred by the chaining rule for derivatives:

$$\frac{\partial G}{\partial \overline{\rho_{s,t}}} = \sum_{e \in I_{s,t}} \frac{\partial G}{\partial \rho_e} \frac{\partial \rho_e}{\partial \overline{\rho_{s,t}}}, \tag{A.1}$$

$$\frac{\partial G}{\partial w_{s,t}} = \sum_{e \in I_{s,t}} \frac{\partial G}{\partial \rho_e} \frac{\partial \rho_e}{\partial w_{s,t}}. \tag{A.2}$$

The derivative $\frac{\partial \rho_e}{\partial \overline{\rho_{s,t}}}$ can be easily computed from Eq. (20):

$$\frac{\partial \rho_e}{\partial \overline{\rho_{s,t}}} = R_{s,t}(u_e, v_e). \tag{A.3}$$

The derivative $\frac{\partial \rho_e}{\partial w_{s,t}}$ is evaluated by explicitly inserting Eq. (2) in Eq. (20). The final expression can be retrieved after few computations:

$$\frac{\partial \rho_e}{\partial w_{s,t}} = \frac{R_{s,t}(u_e, v_e)}{w_{s,t}} (\overline{\rho_{s,t}} - \rho_e). \tag{A.4}$$

Consequently, the sensitivity analysis for the compliance and the volume fraction can be deduced combining Eqs. (A.3) and (A.4) with Eqs. (18) and (19).

Appendix B : Sensitivity Analysis of Constraints

Sensitivity analysis of the minimum member size constraint

Sensitivity of the monotonicity integral $M_{\gamma_i}(\rho)$ with respect to the control points:

$$\begin{aligned}
&\frac{\partial M_{\gamma_i}(\rho)}{\partial \overline{\rho_{s,t}}} = \sum_{j=1}^{N_{\boldsymbol{\gamma}_i}-1} \frac{\partial}{\partial \overline{\rho_{s,t}}} \left(\sqrt{(\rho_{j+1}-\rho_j)^2+\epsilon^2} \right) - \left(\frac{\partial}{\partial \overline{\rho_{s,t}}} \sqrt{(\rho_{N_{\boldsymbol{\gamma}_i}}-\rho_1)^2+\epsilon^2} \right) = \\
&= \sum_{j=1}^{N_{\boldsymbol{\gamma}_i}-1} \frac{(\rho_{j+1}-\rho_j)\left(\frac{\partial \rho_{j+1}}{\partial \overline{\rho_{s,t}}} - \frac{\partial \rho_j}{\partial \overline{\rho_{s,t}}} \right)}{\sqrt{(\rho_{j+1}-\rho_j)^2+\epsilon^2}} - \frac{(\rho_{N_{\boldsymbol{\gamma}_i}}-\rho_1)\left(\frac{\partial \rho_{N_{\boldsymbol{\gamma}_i}}}{\partial \overline{\rho_{s,t}}} - \frac{\partial \rho_1}{\partial \overline{\rho_{s,t}}} \right)}{\sqrt{(\rho_{N_{\boldsymbol{\gamma}_i}}-\rho_1)^2+\epsilon^2}} \\
&= \sum_{j=1}^{N_{\boldsymbol{\gamma}_i}-1} \frac{(\rho_{j+1}-\rho_j)\left(R_{s,t}(u_{j+1},v_{j+1}) - R_{s,t}(u_j,v_j) \right)}{\sqrt{(\rho_{j+1}-\rho_j)^2+\epsilon^2}} + \\
&- \frac{(\rho_{N_{\boldsymbol{\gamma}_i}}-\rho_1)\left(R_{s,t}(u_{N_{\boldsymbol{\gamma}_i}},v_{N_{\boldsymbol{\gamma}_i}}) - R_{s,t}(u_1,v_1) \right)}{\sqrt{(\rho_{N_{\boldsymbol{\gamma}_i}}-\rho_1)^2+\epsilon^2}}.
\end{aligned} \tag{B.1}$$

Sensitivity of the monotonicity integral $M_{\gamma_i}(\rho)$ with respect to the NURBS weights:

$$\begin{aligned}
&\frac{\partial M_{\gamma_i}(\rho)}{\partial w_{s,t}} = \sum_{j=1}^{N_{\boldsymbol{\gamma}_i}-1} \frac{\partial}{\partial w_{s,t}} \left(\sqrt{(\rho_{j+1}-\rho_j)^2+\epsilon^2} \right) - \left(\frac{\partial}{\partial w_{s,t}} \sqrt{(\rho_{N_{\boldsymbol{\gamma}_i}}-\rho_1)^2+\epsilon^2} \right) = \\
&= \sum_{j=1}^{N_{\boldsymbol{\gamma}_i}-1} \frac{(\rho_{j+1}-\rho_j)\left(\frac{\partial \rho_{j+1}}{\partial w_{s,t}} - \frac{\partial \rho_j}{\partial w_{s,t}} \right)}{\sqrt{(\rho_{j+1}-\rho_j)^2+\epsilon^2}} - \frac{(\rho_{N_{\boldsymbol{\gamma}_i}}-\rho_1)\left(\frac{\partial \rho_{N_{\boldsymbol{\gamma}_i}}}{\partial w_{s,t}} - \frac{\partial \rho_1}{\partial w_{s,t}} \right)}{\sqrt{(\rho_{N_{\boldsymbol{\gamma}_i}}-\rho_1)^2+\epsilon^2}} \\
&= \frac{1}{w_{s,t}} \sum_{j=1}^{N_{\boldsymbol{\gamma}_i}-1} \frac{(\rho_{j+1}-\rho_j)\left(\frac{\partial \rho_{j+1}}{\partial \overline{\rho_{s,t}}}(\overline{\rho_{s,t}}-\rho_{j+1}) - \frac{\partial \rho_j}{\partial \overline{\rho_{s,t}}}(\overline{\rho_{s,t}}-\rho_j) \right)}{\sqrt{(\rho_{j+1}-\rho_j)^2+\epsilon^2}} + \\
&- \frac{1}{w_{s,t}} \frac{(\rho_{N_{\boldsymbol{\gamma}_i}}-\rho_1)\left(\frac{\partial \rho_{N_{\boldsymbol{\gamma}_i}}}{\partial \overline{\rho_{s,t}}}(\overline{\rho_{s,t}}-\rho_{N_{\boldsymbol{\gamma}_i}}) - \frac{\partial \rho_1}{\partial \overline{\rho_{s,t}}}(\overline{\rho_{s,t}}-\rho_1) \right)}{\sqrt{(\rho_{N_{\boldsymbol{\gamma}_i}}-\rho_1)^2+\epsilon^2}} = \\
&\frac{\overline{\rho_{s,t}}}{w_{s,t}} \left[\sum_{j=1}^{N_{\boldsymbol{\gamma}_i}-1} \frac{(\rho_{j+1}-\rho_j)\left(\frac{\partial \rho_{j+1}}{\partial \overline{\rho_{s,t}}} - \frac{\partial \rho_j}{\partial \overline{\rho_{s,t}}} \right)}{\sqrt{(\rho_{j+1}-\rho_j)^2+\epsilon^2}} - \frac{(\rho_{N_{\boldsymbol{\gamma}_i}}-\rho_1)\left(\frac{\partial \rho_{N_{\boldsymbol{\gamma}_i}}}{\partial \overline{\rho_{s,t}}} - \frac{\partial \rho_1}{\partial \overline{\rho_{s,t}}} \right)}{\sqrt{(\rho_{N_{\boldsymbol{\gamma}_i}}-\rho_1)^2+\epsilon^2}} \right] + \\
&+ \frac{1}{w_{s,t}} \left[\sum_{j=1}^{N_{\boldsymbol{\gamma}_i}-1} \frac{(\rho_{j+1}-\rho_j)\left(\rho_j \frac{\partial \rho_j}{\partial \overline{\rho_{s,t}}} - \rho_{j+1} \frac{\partial \rho_{j+1}}{\partial \overline{\rho_{s,t}}} \right)}{\sqrt{(\rho_{j+1}-\rho_j)^2+\epsilon^2}} + \right. \\
&\left. - \frac{(\rho_{N_{\boldsymbol{\gamma}_i}}-\rho_1)\left(\rho_1 \frac{\partial \rho_1}{\partial \overline{\rho_{s,t}}} - \rho_{N_{\boldsymbol{\gamma}_i}} \frac{\partial \rho_{N_{\boldsymbol{\gamma}_i}}}{\partial \overline{\rho_{s,t}}} \right)}{\sqrt{(\rho_{N_{\boldsymbol{\gamma}_i}}-\rho_1)^2+\epsilon^2}} \right] = \\
&= \frac{\overline{\rho_{s,t}}}{w_{s,t}} \frac{\partial M_{\gamma_i}(\rho)}{\partial \overline{\rho_{s,t}}} + \frac{1}{w_{s,t}} \left[\sum_{j=1}^{N_{\boldsymbol{\gamma}_i}-1} \frac{(\rho_{j+1}-\rho_j)\left(\rho_j R_{s,t}(u_j,v_j) - \rho_{j+1} R_{s,t}(u_{j+1},v_{j+1}) \right)}{\sqrt{(\rho_{j+1}-\rho_j)^2+\epsilon^2}} + \right. \\
&\left. - \frac{(\rho_{N_{\boldsymbol{\gamma}_i}}-\rho_1)\left(\rho_1 R_{s,t}(u_1,v_1) - \rho_{N_{\boldsymbol{\gamma}_i}} R_{s,t}(u_{N_{\boldsymbol{\gamma}_i}},v_{N_{\boldsymbol{\gamma}_i}}) \right)}{\sqrt{(\rho_{N_{\boldsymbol{\gamma}_i}}-\rho_1)^2+\epsilon^2}} \right].
\end{aligned} \tag{B.2}$$

Sensitivity analysis of the maximum member size constraint

The gradient of the maximum member size constraint is computed here with respect to the NURBS control points and weights:

$$\begin{aligned}
&\frac{\partial g_{d_{max}}}{\partial \overline{\rho_{s,t}}} = \frac{1}{\frac{\pi d_{max}^2}{4}(1-\psi)} \frac{\partial}{\partial \overline{\rho_{s,t}}} \left(\sum_{e=1}^{N_e} \left(\sum_{i \in \Omega_e} \hat{\rho}_i A_i \right)^{\chi} \right)^{\frac{1}{\chi}} = \\
&\frac{\left(\sum_{e=1}^{N_e} \left(\sum_{i \in \Omega_e} \overline{\rho_i} A_i \right)^{\chi} \right)^{\frac{1}{\chi}-1}}{\chi \frac{\pi d_{max}^2}{4}(1-\psi)} \left(\sum_{e=1}^{N_e} \frac{\partial}{\partial \overline{\rho_{s,t}}} \left(\sum_{i \in \Omega_e} \rho_i^{\alpha} A_i \right)^{\chi} \right) = \\
&\frac{\left(\sum_{e=1}^{N_e} \left(\sum_{i \in \Omega_e} \overline{\rho_i} A_i \right)^{\chi} \right)^{\frac{1}{\chi}}}{\frac{\pi d_{max}^2}{4}(1-\psi)} \frac{\left(\sum_{e=1}^{N_e} \left(\sum_{i \in \Omega_e} \rho_i^{\alpha} A_i \right)^{\chi-1} \left(\sum_{i \in \Omega_e} \alpha \rho_i^{\alpha-1} \frac{\partial \rho_i}{\partial \overline{\rho_{s,t}}} A_i \right) \right)}{\sum_{e=1}^{N_e} \left(\sum_{i \in \Omega_e} \overline{\rho_i} A_i \right)^{\chi}} = \\
&\alpha(g_{d_{max}}+1) \frac{\sum_{e=1}^{N_e} \left(\left(\sum_{i \in \Omega_e} \rho_i^{\alpha} A_i \right)^{\chi-1} \left(\sum_{i \in \Omega_e} \rho_i^{\alpha-1} R_{s,t}(u_i, v_i) A_i \right) \right)}{\sum_{e=1}^{N_e} \left(\sum_{i \in \Omega_e} \overline{\rho_i} A_i \right)^{\chi}}.
\end{aligned} \tag{B.3}$$

$$\begin{aligned}
&\frac{\partial g_{d_{max}}}{\partial w_{s,t}} = \alpha(g_{d_{max}}+1) \frac{\sum_{e=1}^{N_e} \left(\left(\sum_{i \in \Omega_e} \rho_i^{\alpha} A_i \right)^{\chi-1} \left(\sum_{i \in \Omega_e} \rho_i^{\alpha-1} \frac{\partial \rho_i}{\partial w_{s,t}} A_i \right) \right)}{\sum_{e=1}^{N_e} \left(\sum_{i \in \Omega_e} \overline{\rho_i} A_i \right)^{\chi}} = \\
&= \alpha(g_{d_{max}}+1) \frac{\sum_{e=1}^{N_e} \left(\left(\sum_{i \in \Omega_e} \rho_i^{\alpha} A_i \right)^{\chi-1} \left(\sum_{i \in \Omega_e} \rho_i^{\alpha-1} \frac{\partial \rho_i}{\partial \overline{\rho_{s,t}}} \frac{\overline{\rho_{s,t}} - \rho_i}{w_{s,t}} A_i \right) \right)}{\sum_{e=1}^{N_e} \left(\sum_{i \in \Omega_e} \overline{\rho_i} A_i \right)^{\chi}} = \\
&= \frac{\overline{\rho_{s,t}}}{w_{s,t}} \alpha(g_{d_{max}}+1) \frac{\sum_{e=1}^{N_e} \left(\left(\sum_{i \in \Omega_e} \rho_i^{\alpha} A_i \right)^{\chi-1} \left(\sum_{i \in \Omega_e} \rho_i^{\alpha-1} \frac{\partial \rho_i}{\partial \overline{\rho_{s,t}}} A_i \right) \right)}{\sum_{e=1}^{N_e} \left(\sum_{i \in \Omega_e} \overline{\rho_i} A_i \right)^{\chi}} + \\
&- \frac{1}{w_{s,t}} \alpha(g_{d_{max}}+1) \frac{\sum_{e=1}^{N_e} \left(\left(\sum_{i \in \Omega_e} \rho_i^{\alpha} A_i \right)^{\chi-1} \left(\sum_{i \in \Omega_e} \rho_i^{\alpha} \frac{\partial \rho_i}{\partial \overline{\rho_{s,t}}} A_i \right) \right)}{\sum_{e=1}^{N_e} \left(\sum_{i \in \Omega_e} \overline{\rho_i} A_i \right)^{\chi}} = \\
&\frac{\overline{\rho_{s,t}}}{w_{s,t}} \frac{\partial g_{d_{max}}}{\partial \overline{\rho_{s,t}}} - \frac{\alpha(g_{d_{max}}+1)}{w_{s,t}} \frac{\sum_{e=1}^{N_e} \left(\left(\sum_{i \in \Omega_e} \rho_i^{\alpha} A_i \right)^{\chi-1} \left(\sum_{i \in \Omega_e} \rho_i^{\alpha} R_{s,t}(u_i, v_i) A_i \right) \right)}{\sum_{e=1}^{N_e} \left(\sum_{i \in \Omega_e} \overline{\rho_i} A_i \right)^{\chi}}.
\end{aligned} \tag{B.4}$$

Sensitivity analysis of the local curvature radius constraint

The gradient of the local curvature radius is computed with respect to the control points and to the weights. Let us write again Eq. (50) in a more convenient form:

$$r = -\frac{1}{WH} \frac{r_N}{r_D}. \tag{B.5}$$

Thus, the derivatives write

$$\frac{\partial r}{\partial \overline{\rho_{s,t}}} = r \left(\frac{1}{r_N} \frac{\partial r_N}{\partial \overline{\rho_{s,t}}} - \frac{1}{r_D} \frac{\partial r_D}{\partial \overline{\rho_{s,t}}} \right), \tag{B.6}$$

$$\frac{\partial r}{\partial w_{s,t}} = r \left(\frac{1}{r_N} \frac{\partial r_N}{\partial w_{s,t}} - \frac{1}{r_D} \frac{\partial r_D}{\partial w_{s,t}} \right). \tag{B.7}$$

The complete expression of Eqs. (B.6) and (B.7) are not provided here for sake of brevity; anyway the reader can easily deduce them by using the following formulae to compute the derivatives of each term. They are deduced from the results of Appendix A:

$$\frac{\partial}{\partial\overline{\rho_{s,t}}}\left(\frac{\partial\rho}{\partial u}\right)=\frac{\partial R_{s,t}}{\partial u}, \tag{B.8}$$

$$\frac{\partial}{\partial\overline{\rho_{s,t}}}\left(\frac{\partial\rho}{\partial v}\right)=\frac{\partial R_{s,t}}{\partial v}, \tag{B.9}$$

$$\frac{\partial}{\partial\overline{\rho_{s,t}}}\left(\frac{\partial^2\rho}{\partial u^2}\right)=\frac{\partial^2 R_{s,t}}{\partial u^2}, \tag{B.10}$$

$$\frac{\partial}{\partial\overline{\rho_{s,t}}}\left(\frac{\partial^2\rho}{\partial u\partial v}\right)=\frac{\partial^2 R_{s,t}}{\partial u\partial v}, \tag{B.11}$$

$$\frac{\partial}{\partial\overline{\rho_{s,t}}}\left(\frac{\partial^2\rho}{\partial v^2}\right)=\frac{\partial^2 R_{s,t}}{\partial v^2}, \tag{B.12}$$

$$\frac{\partial}{\partial w_{s,t}}\left(\frac{\partial\rho}{\partial u}\right)=\frac{\overline{\rho_{s,t}}-\rho}{w_{s,t}}\frac{\partial R_{s,t}}{\partial u}-\frac{R_{s,t}}{w_{s,t}}\frac{\partial\rho}{\partial u}, \tag{B.13}$$

$$\frac{\partial}{\partial w_{s,t}}\left(\frac{\partial\rho}{\partial v}\right)=\frac{\overline{\rho_{s,t}}-\rho}{w_{s,t}}\frac{\partial R_{s,t}}{\partial v}-\frac{R_{s,t}}{w_{s,t}}\frac{\partial\rho}{\partial v}, \tag{B.14}$$

$$\frac{\partial}{\partial w_{s,t}}\left(\frac{\partial^2\rho}{\partial u^2}\right)=\frac{1}{w_{s,t}}\left((\overline{\rho_{s,t}}-\rho)\frac{\partial^2 R_{s,t}}{\partial u^2}-2\frac{\partial R_{s,t}}{\partial u}\frac{\partial\rho}{\partial u}-R_{s,t}\frac{\partial^2\rho}{\partial u^2}\right), \tag{B.15}$$

$$\frac{\partial}{\partial w_{s,t}}\left(\frac{\partial^2\rho}{\partial u\partial v}\right)=\frac{1}{w_{s,t}}\left((\overline{\rho_{s,t}}-\rho)\frac{\partial^2 R_{s,t}}{\partial u\partial v}-\frac{\partial R_{s,t}}{\partial u}\frac{\partial\rho}{\partial v}-\frac{\partial R_{s,t}}{\partial v}\frac{\partial\rho}{\partial u}-R_{s,t}\frac{\partial^2\rho}{\partial u\partial v}\right), \tag{B.16}$$

$$\frac{\partial}{\partial w_{s,t}}\left(\frac{\partial^2\rho}{\partial v^2}\right)=\frac{1}{w_{s,t}}\left((\overline{\rho_{s,t}}-\rho)\frac{\partial^2 R_{s,t}}{\partial v^2}-2\frac{\partial R_{s,t}}{\partial v}\frac{\partial\rho}{\partial v}-R_{s,t}\frac{\partial^2\rho}{\partial v^2}\right). \tag{B.17}$$

References

[1] M. Bendsoe and N. Kikuchi. Generating optimal topologies in structural design using a homogenization method. *Computer Methods in Applied Mechanics and Engineering*, 71:197–224, 1988.

[2] M. Bendsoe and O. Sigmund. *Topology Optimization - Theory, Methods and Applications*. Springer, 2003.

[3] J. K. Guest, J. H. PrÃĭvost, and T. Belytschko. Achieving minimum length scale in topology optimization using nodal design variables and projection functions. *Numerical Methods in Engineering*, 61:238–254, 2004.

[4] F. Wang, B. S. Lazarov, and O. Sigmund. On projection methods, convergence and robust formulations in topology optimization. *Structural and Multidisciplinary Opimization*, 43(6):767–784, 2011.

[5] J. K. Guest. Imposing maximum length scale in topology optimization. *Structural and Multidisciplinary Opimization*, 37:463–473, 2009.

[6] O. Sigmund. A 99 line topology optimization code written in matlab. *Structural and Multidisciplinary Opimization*, 21:120–127, 2001.

[7] J. A. Sethian. *Level Set Methods and Fast Marching Methods - Evolving interfaces in computational geometry, fluid mechanics, computer vision, and materials science.* Cambridge University Press, 1999.

[8] M. J. de Ruiter and F. van Keulen. Topology optimization using a topology description function. *Structural and Multidisciplinary Optimization*, 26:406–416, 2004.

[9] G. Allaire, F. Jouve, and A. M. Toader. Structural optimization using sensitivity analysis and a level-set method. *Jounral of Computational Physics*, 194:363–393, 2004.

[10] N. P. van Dijk, K. Maute, M. Langelaar, and F. van Keulen. Level-set methods for structural topology optimization: a review. *Structural and Multidisciplinary Optimization*, 48:437–472, 2013.

[11] S. Y. Wang and M. Y. Wang. Radial basis functions and level set method for structural topology optimization. *International Journal for Numerical Method in Engineering*, 65(12):2060–2090, 2006.

[12] Z. Luo, L. Tong, M. Y. Wang, and S. Wang. Shape and topology optimization of compliant mechanisms using a parameterization level set method. *Journal of Computational Physics*, 227:680–705, 2007.

[13] Z. Luo, L. Tong, and Z. Kang. A level set method for structural shape and topology optimization using radial basis functions. *Computers and Structures*, 87:425–434, 2009.

[14] Y. Wang and D. J. Benson. Geometrically constrained isogeometric parametrized level-set based topology optimization via trimmed elements. *Frontiers of Mechanical Engineering*, 11(4):328–343, 2016.

[15] T. Yamada, K. Izui, S. Nishiwaki, and A. Takezawa. A topology optimization method based on the level set method incorporating a fictitious interface energy. *Computer Methods in Applied Mechanics and Engineering*, 199:2876âĂŞ2891, 2010.

[16] X. Qian. Topology optimization in b-spline space. *Computer Methods in Applied Mechanics and Engineering*, 265:15–35, 2013.

[17] *OptiStruct 13.0 Reference Guide*, 2014.

[18] *SIMUILIA Tosca Structure Documentation 8.0*, 2013.

[19] T.A. Poulsen. A new scheme for imposing a minimum length scale in topology optimization. *International Journal for Numerical Methods in Engineering*, 57:741–760, 2003.

[20] M. Zhou, B. S. Lazarov, F. Wang, and O. Sigmund. Minimum length scale in topology optimization by geometric constraints. *Computer Methods in Applied Mechanics and Engineering*, 293:266–282, 2015.

[21] O. Sigmund. Manufacturing tolerant topology optimization. *Acta Mechanica Sinica*, 25:227–239, 2009.

[22] X. Guo, W. Zhang, and W. Zhong. Explicit feature control in structural topology optimization via level set method. *Computer Methods in Applied Mechanics and Engineering*, 272:354–378, 2014.

[23] G. Allaire, F. Jouve, and G. Michailidis. Thickness control in structural optimization via a level set method. *Structural and Multidisciplinary Optimization*, 53(6):1349–1382, 2016.

[24] G. Costa, M. Montemurro, and J. Pailhès. A nurbs-based topology optimisation method including additive manufacturing constraints. In *7th International Conference on Mechanics and Materials in Design*, 2017.

[25] L. Piegl and W. Tiller. *The NURBS book*. Springer-Verlag, Berlin, Heidelberg, New York, 1997.

[26] P. Mercelis and J. P. Kruth. Residual stresses in selective laser sintering and selective laser melting. *Rapid Prototyping Journal*, 12:254–265, 2006.

[27] R. Goldman. Curvature formulas for implicit curves and surfaces. *Computer Aided Geometric Design*, 22:632–658, 2005.

[28] G. Kreisselmeier and R. Steinhauser. Systematic control design by optimizing a vector performance index. *IFAC Proceedings Volumes*, 12(7):113 – 117, 1979.

[29] K. Svanberg. The method of moving asymptotes - a new method for structural optimization. *International Journal for Numerical Methods in Engineering*, 24:359–373, 1987.

[30] *Optimization Toolbox User's Guide*. The MathWorks Inc, 3 Apple Hill Drive, Natick, September 2011.

[31] J. Nocedal and S. J. Wright. *Numerical Optimization*. Springer Verlag, second edition, 2006.

[32] F. Auricchio, L. BeirÃčo da Veiga, T. J. R. Hughes, A. Reali, and G. Sangalli. Isogeometric collocation methods. *Mathematical Models and Methods in Applied Sciences*, 20(11):2075–2107, 2010.

[33] Ansys. *ANSYS Mechanical APDL Basic Analysis Guide. Release 16.0*. ANSYS, Inc., Southpointe, 275 Technology Drive, Canonsburg, PA 15317, 2014.